博士論文

Innovative modeling and simulation approach considering the time-dependent pharmacologic activity in translational research among non-clinical and clinical studies.

（非臨床試験と臨床試験の橋渡し研究における時間依存的な薬効を考慮した革新的な **modeling & simulation** アプローチ）

高田　祥世

北海道大学大学院生命科学院

平成 **29** 年 **3** 月

CONTENTS

ABBREVIATIONS

Abbreviations	Description
ABC	accelerated blood clearance
ACV	acyclovir
ALB	albumin
ALP	alkaline phosphatase
ALT	alanine aminotransferase
AST	aspartate transaminase
AUC	area under the concentration–time curve
Amenamevir	international non-proprietary name for ASP2151.
BILI	total bilirubin
BLQ	lower limit of quantitation
BUN	blood urea nitrogen
CHE	cholesteryl hexadecyl ether
CHO	cholesterol
CI	confidence interval
CL/F	apparent total clearance
CV	coefficient of variation
CWRES	conditional weighted residuals
C_{min}	minimum effective concentration
Cr	creatinine
DDS	drug delivery system
Dox	doxorubicin
EC_{50}	michaelis constant
ECMP	monophosphate derivative of ECyd
ECTP	triphosphate derivative of ECyd
ECyd	1-(3-C-ethynyl-β-D-ribo-pentofuranosyl) cytosine (3'-ethynylcytidine)
EPC	egg yolk phosphatidylcholine
E_{max}	maximum efficacy
FBS	fetal bovine serum
FDA	food and drug administration
FOCE-INTERACTION	first-order conditional estimation with interaction
HCT	hematocrit
HEF	human embryonic fibroblast
HGB	hemoglobin
HSV-1	herpes simplex virus type 1
HSV-2	herpes simplex virus type 2
Ht	height
IC_{50}	inhibitory concentration
IRB	institutional review board
LC-MS/MS	liquid chromatography-tandem mass spectrometry
LLOQ	The lower limit of quantification
M & S	Modeling and Simulation
PCR	polymerase chain reaction
PD	pharmacodynamic
PEG	polyethylene glycol
PK	pharmacokinetic
PLT	platelet
PPK	population pharmacokinetics
QOL	quality of life
RBC	red blood cell
RES	residual
RSE	residual standard error

Ret	reticulocyte counts
TP	total protein
UCK2	uridine-cytidine kinase 2
V/F	apparent distribution volume
VACV	valacyclovir
VZV	varicella-zoster virus
WBC	white blood cell
WGT	weight
k_a	absorption rate constant
l.l.d.	log-likelihood difference
p.o.	per os: oral administration
t_{50}	50% inhibitory time

GENERAL INTRODUCTION

In translational research in drug development, correctly evaluate the characteristics of the drug under development by utilizing the non-clinical and clinical trial data obtained in the development process, it can contribute to the rapid and efficient development as a result. Although the evaluation of drugs has various purposes, it is essential to develop a highly accurate pharmacokinetic / disease model. Specifically, research methods classified as so-called Pharmacometrics, such as population pharmacokinetics (PPK), exposure / pharmacodynamic analysis, Pharmacodynamic (PD) model construction, etc. are incorporated in the drug development process. Modeling and Simulation (M & S) technique is used to explain with an appropriate mathematical model and makes future prediction.

In this study, I focused on not only the drug concentration but also the drug depending on the time from the administration (time dependency of efficacy). I investigated with a view to comprehensively examining the time dependency of efficacy by constructing a model based on nonclinical *in vitro, in vivo* and clinical study data.

The results were described over two chapters.

In Chapter 1, I investigated the dependence of efficacy based on PK model of *in vivo* study of new antitumor drug ECyd, and examined enhancement of efficacy by appropriate design of drug carrier.

In Chapter 2, I conducted PPK and PK / PD analysis for genital herpes patients in study of a novel antiviral drug, Amenamevir. Additionally, integrated PK/PD model study combining the nonclinical data was conducted to consider the time dependency of Amenamevir efficacy.

1 CHAPTER1

1.1 PK-PD modeling of 1-(3-C-ethynyl-D-ribo-pentofuranosyl)cytosine and the enhanced antitumor effect of its phospholipid derivatives in long-circulating liposomes

1.1.1 Introduction

Antitumor drugs are classified into two groups based on their dose-dependencies[1-3]. One is a concentration-dependent drug group, which includes alkylating agents, intercalators and platinum derivatives (type I). Their cytotoxic effect depends on both concentration and exposure time, namely, on the area under the concentration–time curve (AUC). Thus, short exposure to these drugs at high concentration, and long exposure at low concentration, results in similar cytotoxicity. The other group is the exposure time-dependent drug group, which includes antimetabolites and vinca alkaloids (type II). Their cytotoxicity requires a certain exposure period, and short exposure at high concentration does not exert sufficient antitumor activity. Based on studies by Sugiyama's group, cell-cycle independent and dependent antitumor drugs are classified into type I and type II groups, respectively[2,3].

The type I antitumor drugs can be expected to be more effective when a drug delivery system (DDS) increases their AUC. Liposomes are a candidate for useful carriers that encapsulate water-soluble drugs into the aqueous phase and lipid-soluble drugs into the lipid membrane. Polyethylene glycol (PEG)ylation can dramatically prolong liposome circulation time in blood by preventing the absorption of liposomes onto opsonins, serum proteins [4-6]. Unmodified liposomes disappear from blood circulation due to entrapment by reticuloendothelial system organs, such as liver and spleen, before they reach tumor tissue. On the other hand, PEGylated long-circulating liposomes can deliver antitumor drugs to tumor tissue by escaping from recognition by opsonins in blood. The long circulation of the PEG-liposomes is also expected to enhance the antitumor effects of type II drugs, since they can be released for a longer period. Doxorubicin (Dox) and vincristine, AUC-dependent type I and AUC-independent type II antitumor drugs,

respectively, have been shown to have enhanced activity after encapsulation into long-circulating liposomes[7,8]. An antitumor nucleoside, 1-(3-C-ethynyl-β-D-ribo-pentofuranosyl) cytosine (3'-ethynylcytidine, ECyd) (Figure 1- 1), exerts its cytotoxic effect by transcription inhibition and apoptosis induction[9-12]. ECyd is phosphorylated by uridine-cytidine kinase 2 (UCK2) to form the monophosphate derivative (ECMP), and subsequent phosphorylation reactions yield the actual drug, ECTP, the triphosphate derivative [13,14]. The action mechanism of ECyd (ECTP) is inhibition of RNA polymerases, resulting in the disturbance of various cellular events. Thus, ECyd is thought to be independent of the cell cycle and a type I drug (AUC-dependent). Thus, the encapsulation of ECyd into long-circulating liposomes could enhance its antitumor effect as that of the AUC-dependent type I antitumor drug, Dox.

To design excellent carriers of antitumor drugs, analysis of their antitumor effects based on the physiological model is important. However, such DDS design has rarely been reported. Previously, one of the authors (H. H.) analyzed liposomal Dox based on the model and found that optimization of its release rate is an important factor in the enhancement of the antitumor effect [15,16]. In this study, the antitumor effect of ECyd was analyzed *in vitro* and *in vivo*. The antitumor effect of ECyd encapsulated in long-circulating liposomes was also examined. Based on *in vivo* pharmacokinetic (PK)–pharmacodynamic (PD) analyses, a physiological model that could explain its *in vivo* antitumor effect quantitatively was proposed. The model suggested that ECyd followed a time-dependent mechanism of action *in vivo* (in contrast to *in vitro*), and that the availability of ECyd in tumor tissue is highly important. To increase the availability of ECyd, its phospholipid derivatives were synthesized and encapsulated into long-circulating liposomes. These liposomes successfully increased the antitumor effect. These

results indicate that the design of carriers of antitumor drugs based on their physiological models is highly important.

1.1.2 Materials and methods

1.1.2.1 Materials

ECyd was synthesized as described previously [9]. Colon 26 cells were provided by Taiho Pharmaceutical Co. (Tokyo, Japan).

1.1.2.2 Chemical synthesis of phospholipid derivatives of ECyd

A mixture of a solution of 3-sn-diacylphosphatidylcholine (dipalmitoyl-, distearoyl-, or dioleoyl-phosphatidylcholine, 3.4 mmol) in $CHCl_3$ (50 mL), phospholipase D (PLDP, Asahi Kasei Co., Tokyo, Japan) (60 mg, 10,800 units) and a solution of ECyd (4.54 g, 17 mmol) in sodium acetate buffer (pH 4.5, 200 mM, 25 ml) was stirred at 40 °C for 2.5 h. $CHCl_3$ (60 mL), MeOH (60 mL) and water (10 mL) were added to the resulting mixture, and the organic layer was evaporated. The residue was purified on a silica gel column (33–50% MeOH in $CHCl_3$). The fractions containing the desired product were collected and evaporated.

The residue was dissolved in a mixture of $CHCl_3 - MeOH - water$ (10/5/1), loaded on a WK-20 (Na+ form) column and eluted using the same mixed solvent. The eluate was evaporated to give DPPECyd, DSPECyd, or DOPECyd as a sodium salt. DPPECyd: yield 52%; mp 206–208°C (decomp.); ^{1}H NMR ($CDCl_3 - CD_3OD$ (3:1)) 7.96 (d, 1H, H-6, *J* = 7.6 Hz), 5.94 (d, 1H, ECyd H-1', *J* = 5.1 Hz), 5.91 (d, 1H, ECyd H-5, *J* = 7.6 Hz), 5.23 (m, 1H, glycerol H-2), 4.41 (dd, 1H, H-5'a, *J* = 2.9, 11.7 Hz), 4.2–4.3 (m, 4H, H-2', H-5'b, glycerol CH_2), 4.00 (t, 2H, *J* = 5.7 Hz, glycerol CH_2), 3.84 (m, 1H, ECyd H-4'), 2.78 (s, 1H, ECyd 3'-ethynyl), 2.28–2.35 (m, 4H, $COCH_2 \times 2$), 1.59 (m, 4H, $COCH_2CH_2 \times 2$), 1.26 (m, 48H, pal-$CH_2 \times 2$), 0.88 (t, 6H, J = 6.7 Hz, pal-$CH_3 \times 2$); FAB-MS m/z 920

(MH+). Anal. calcd. for $C_{46}H_{79}N_3NaO_{12}P \cdot 1/2H_2O$: C, 59.47; H, 8.68; N, 4.52. Found: C, 59.27; H, 8.60; N, 4.03. DSPECyd: yield 45%; mp 222–226 °C (decomp.); ^{1}H NMR ($CDCl_3 - CD_3OD$ (3:1)) 7.98 (d, 1H, H-6, *J* = 7.6 Hz), 5.94 (d, 1H, ECyd H-1', *J* = 4.9 Hz), 5.92 (d, 1H, ECyd H-5, *J* = 7.6 Hz), 5.23 (m, 1H, glycerol H-2), 4.41 (dd, 1H, H-5'a, *J* = 3.2, 12.0 Hz), 4.19–4.26 (m, 4H, H-2', H-5'b, glycerol CH_2), 4.00 (t, 2H, *J* = 5.6 Hz, glycerol CH_2), 3.85 (br, 1H, ECyd H-4'), 2.78 (s, 1H, ECyd 3'-ethynyl), 2.28–2.35 (m, 4H, $COCH_2 \times 2$), 1.59 (m, 4H, $COCH_2CH_2 \times 2$), 1.26 (m, 56H, stearoyl-CH_2), 0.88 (t, 6H, *J* = 6.7 Hz, stearoyl $CH_3 \times 2$); FAB-MS m/z 976 (MH+). Anal. calcd. for $C_{50}H_{87}N_3NaO_{12}P$: C, 61.52; H, 8.98; N, 4.30. Found: C, 61.39; H, 8.75; N, 4.49. DOPECyd: yield 56%; mp 208–227 °C (decomp.); ^{1}H NMR ($CDCl_3 - CD_3OD$ (3:1)) 7.94 (d, 1H, H-6, *J* = 7.6 Hz), 5.94 (d, 1H, ECyd H-1', *J* = 4.9 Hz), 5.91 (d, 1H, ECyd H-5, *J* = 7.6 Hz), 5.30–5.37 (m, 4H, olefinic), 5.22–5.35 (m, 1H, glycerol H-2), 4.41 (dd, 1H, H-5'a, *J* = 3.4, 12.0 Hz), 4.16–4.26 (m, 4H, H-2', H-5'b, glycerol CH_2), 4.00 (t, 2H, J = 5.7 Hz, glycerol CH_2), 3.69 (br, 1H, ECyd H-4'), 2.76 (s, 1H, ECyd 3'-ethynyl), 2.28–2.35 (m, 4H, $COCH_2 \times 2$), 1.99–2.02 (8H, m, oleoyl-$CH_2 \times 4$), 1.57–1.61 (m, 4H, $COCH_2CH_2 \times 2$), 1.24–1.45 (m, 40H, oleoyl-$CH_2 \times 20$), 0.88 (t, 6H, *J* = 6.8 Hz, oleoyl $CH_3 \times 2$); FAB-MS (neg.) m/z 948 (M–Na)-. Anal. calcd. for $C_{50}H_{83}N_3NaO_{12}P$: C, 61.77; H, 8.60; N, 4.32. Found: C, 61.55; H, 8.50; N, 4.33.

1.1.2.3 Preparation of liposomes

Liposomes were composed of distearoylphosphatidylcholine, cholesterol, dicetyl phosphate, and 1,2-distearoyl-sn-glycero-3-phosphoethanolamine-N- [lo(polyethylene glycol)-3000] (6:3:1:1 molar ratio). Liposomes encapsulating ECyd or $[^3H]$ ECyd were prepared by the hydration method [17] followed by extrusion (the Mini-Extruder, Avanti polar lipids) through polycarbonate membrane filters (Nuclepore) of 200 nm and 100 nm, twenty-one times for each pore size. The unencapsulated drug was removed by dialysis

against saline six times. The encapsulation ratio, determined by radioactivity after the final dialysis, was 5%. Liposomes labeled with [^{3}H] cholesteryl hexadecyl ether (CHE) were prepared by a similar procedure without the dialysis. Liposomes containing a phospholipid derivative of ECyd were composed of egg yolk phosphatidylcholine (EPC), cholesterol, dicetyl phosphate, and 1,2-distearoyl-sn-glycero-3-phosphoethanolamine-N-[methoxy(polyethylene glycol)-3000] (7:2:1:1 molar ratio). The encapsulation ratio of the phospholipid derivatives was hypothesized as 100%.

1.1.2.4 *In vitro* chemosensitivity test

The growth-inhibitory effects of ECyd on mouse colorectal carcinoma cells were determined by colorimetric assay. Colon 26 cells (5.0×10^4 cells/well) were grown in RPMI-1640 medium with 10% fetal calf serum (100 µl) under a 5% CO_2/95% air atmosphere at 37 °C. After 24 hrs, the cells were exposed to ECyd at various concentrations for the time periods indicated. The medium containing ECyd was replaced every 12 hr. After exposure to the drug, cells were washed with the medium twice, and then incubated in 100 µl of the medium at 37 °C up to 48 hr after exposure initiation. The medium was removed, 110 µl of TetraColor One (Seikagaku Co., Tokyo, Japan) was added to each well, and the cell cultures were incubated at 37 °C for 3 hr. The absorbance of each well was measured at 450 nm using a Benchmark Plus (BIO-RAD, Hercules, California, USA). The 50% inhibitory concentration (IC_{50}) was determined from the dose–response curve.

1.1.2.5 *In vivo* antitumor activity

Colon 26 cells (1×10^7 cells/mouse) were transplanted hypodermically into 5-week-old male BALB/c mice on day 0. ECyd, or liposomes encapsulating ECyd, were intravenously administered to tumor-bearing BALB/c mice on days 5 and 10, or on day 8. Tumors were collected on day 15 from ether-anesthetized mice, and the averaged

volumes of tumors in the administered mice were calculated. The inhibition ratio (IR) was calculated using the equation below:

$$\mathrm{IR}(\%) = \left(1 - \frac{\text{mean tumor volume of treated group}}{\text{mean tumor volume of control group}}\right) \times 100 \qquad \text{(eq. 1)}$$

1.1.2.6 Pharmacokinetics of free ECyd

Colon 26 cells (1×10^7 cells/mouse) were transplanted hypodermically into 5-week-old male BALB/c mice on day 0. [^{3}H]ECyd was intravenously administered to tumor-bearing BALB/c mice. Blood and tumor were collected from ether-anesthetized mice. 100 µl of blood and 1 ml of Soluene-350 (Perkin Elmer, Wellesley, MA, USA) were mixed and incubated at 50 °C for 15–30 min, decolorized with 30% hydrogen peroxide, and mixed with aqueous counting scintillant (Hionic-Fluor, Perkin Elmer). The mixture was kept at 4 °C overnight. 100–200 mg of the collected tumor was solubilized in 1 ml of Soluene-350 by incubation at 50 °C for 2–4 hrs, and mixed with Hionic-Fluor. The mixture was kept at 4 °C overnight. ^{3}H-radioactivity was counted on a liquid scintillation counter.

1.1.2.7 Pharmacokinetics of liposomes

Liposomes labeled with [^{3}H]CHE or liposomes encapsulating [^{3}H]ECyd were intravenously administered to tumor-bearing BALB/c mice, and the time courses of the concentration in blood and the amount in tumor were measured as described above.

1.1.2.8 Computational simulations

The pharmacokinetic data were analyzed using SAAM II (SAAM Institute, Seattle, WA, USA) and Stella (High Performance Systems, Hanover, NH, USA) software. The mass balance equations for free ECyd (Scheme 1A) are as follows:

$$\text{Blood: } V_{b,f}\frac{dC_{b,f}}{dt} = k_{21}X_{ti,f} + k_{31}V_{tu,f}C_{tu,f} - (k_{10} + k_{12} + k_{13})V_{b,f}C_{b,f} \qquad \text{(eq. 2)}$$

Tumor: $V_{tu,f}\frac{dC_{tu,f}}{dt} = k_{13}V_{b,f}C_{b,f} - k_{31}V_{tu,f}C_{tu,f}$ (eq. 3)

Tissue: $\frac{dX_{ti,f}}{dt} = k_{12}V_{b,f}C_{b,f} - k_{21}X_{ti,f}$ (eq. 4)

The mass balance equations for free ECyd upon liposomal ECyd injection (Scheme 1A) are as follows:

Blood: $V_{b,f}\frac{dC_{b,f}}{dt} = k_{21}X_{ti,f} + k_{31}V_{tu,f}C_{tu,f} - (k_{10} + k_{12} + k_{13})V_{b,f}C_{b,f} + (k_{rel,blood,fast} + k_{rel,blood,slow})V_{b,lipo}C_{b,lipo}$ (eq. 5)

Tumor: $V_{tu,f}\frac{dC_{tu,f}}{dt} = k_{13}V_{b,f}C_{b,f} - k_{31}V_{tu,f}C_{tu,f} + k_{rel,tumor}V_{tu,lipo}C_{tu,lipo}$ (eq. 6)

Tissue: $\frac{dX_{ti,f}}{dt} = k_{12}V_{b,f}C_{b,f} - k_{21}X_{ti,f}$

The mass balance equations for liposomal ECyd upon liposomal ECyd injection (Scheme 1A) are as follows:

Blood: $V_{b,lipo}\frac{dC_{b,lipo}}{dt} = k_{54}V_{tu,lipo}C_{tu,lipo} - (k_{40} + k_{45} + k_{rel,blood,fast} + k_{rel,blood,slow})V_{b,lipo}C_{b,lipo}$ (eq. 7)

Tumor: $V_{tu,lipo}\frac{dC_{tu,lipo}}{dt} = k_{45}V_{b,lipo}C_{b,lipo} - (k_{54} + k_{rel,tumor})V_{tu,lipo}C_{tu,lipo}$ (eq. 8)

$V_{b,f}$ and $V_{tu,f}$ represent the volumes of distribution for free ECyd in the blood and tumor compartments, respectively. $V_{b,lipo}$ and $V_{tu,lipo}$ represent the volumes of distribution for liposomal ECyd in the blood and tumor compartments, respectively. $C_{b,f}$, $C_{tu,f}$, $C_{b,lipo}$ and $C_{tu,lipo}$ represent the free and liposomal ECyd concentrations in the blood and tumor compartments. $X_{ti,f}$ represents amount of free ECyd in the tissue compartment. k_{10} and k_{40} represent the elimination constants for free and liposomal ECyd, respectively. k_{12}, k_{13}, k_{21}, k_{31}, k_{45} and k_{54} represent the distribution rate constants. $k_{rel,tumor}$ represents the ECyd release rate constant in the tumor compartment. $k_{rel,blood,fast}$ and $k_{rel,blood,slow}$

represent the fast and slow ECyd release rate constants in the blood compartment, respectively.

1.1.3 Results

1.1.3.1 AUC-dependence of the cytotoxic effects of ECyd *in vitro*

The cytotoxic effects of ECyd on mouse colorectal carcinoma cells (Colon 26 cells) were determined by MTT assay. Exposure time was altered (4, 12, 24 and 48 h), and IC_{50} values were determined for each exposure time. As shown in Table 1- 3, the IC_{50} values decreased as the treatment time increased. AUC, the product of the exposure time and the IC_{50} values obtained, were similar for each condition. These results were in agreement with the hypothesis that ECyd is a cell cycle-independent antitumor drug, since ECyd inhibits RNA synthesis. In addition, these results suggest that the antitumor effect of ECyd would be independent of the administration schedule *in vivo*.

1.1.3.2 Pharmacokinetics of ECyd

[^{3}H] ECyd was intravenously administered to tumor-bearing BALB/c mice and radioactivity in blood and tumors was determined (Figure 1- 3A and B). The amounts in blood and tumors, relative to the injected [^{3}H] ECyd, were similar when various amounts of [^{3}H] ECyd were injected (data not shown), indicating the linearity of the drug disposition under the experimental conditions. Importantly, ECyd was cleared rapidly from blood.

1.1.3.3 AUC-independence of the antitumor effects of ECyd *in vivo*

Various doses of ECyd were then intravenously administered to tumor-bearing BALB/c mice on days 5 and 10 (double administration), or day 8 (single administration). Tumors were collected on day 15 and the IR values were determined. In contrast to the expectations based on the *in vitro* cytotoxic effect (Table 1- 3), the antitumor effect of ECyd was schedule-dependent. As shown in Table 1- 1 (Experiment 1) and Figure 1- 4A,

double administration of ECyd inhibited tumor growth more effectively than single administration of the same total dose of ECyd. For example, the IR of a single 3.0 mg/kg injection was 48%, and that of double 1.5 mg/kg injections was 86%. Since the PK of ECyd was linear under the experimental conditions, as described above, these results indicate type II-like AUC-independence of the antitumor effects of ECyd *in vivo*.

1.1.3.4 PK–PD modeling ofECyd

PK parameters were obtained by curve-fitting based on the three-compartment model shown in Scheme 1A (see "Free ECyd") and the actual ECyd dose data in blood and tumor tissue (Figure 1- 3A and B), according to the equations described in the Materials and Methods section. The PK parameters obtained are shown in Table 1- 2. The linearity of the ECyd disposition under these conditions was observed, and the same values of the parameters were used in the following simulations. To explain the fact that the antitumor effect of ECyd was AUC-dependent *in vitro* and AUC-independent *in vivo* (Table 1- 3 and Table 1- 1, Experiment 1), the presence of a minimum effective concentration (C_{min}) was introduced as a new parameter. I hypothesized that ECyd can exert antitumor effect only when free concentration of ECyd exceeds the C_{min} in tumor tissue (Scheme 1B). However, since we could not measure the C_{min}, I estimated the C_{min} based on the simulation as explained below. The putative C_{min} value was changed in the simulation, and the effective time within which the ECyd concentration in the tumor was above C_{min} was calculated for each C_{min} value. I then examined the curve-fitting of calculated effective times and the actually observed IR values, using the following equation

$$IR = \frac{E_{max} \times t^r}{t_{50}^r + t^r} \qquad \text{(eq. 9)}$$

where E_{max}, t, and t_{50} represent the maximum efficacy (set as 100%), effective time, and 50% inhibitory time, respectively. In the case of double administration, the calculated

effective time was doubled. As shown in Figure 1- 4B, the IR data of the single and double administration experiments fitted well as the function of effective time when C_{min} was set at 61.1 fmol/g (the t_{50} and r values were calculated as 147.5 hr and 2.9, respectively). Thus, the threshold value C_{min} could well explain the *in vivo* antitumor effects of ECyd.

1.1.3.5 The antitumor effects of liposomal ECyd *in vivo*

The results shown above suggest that the antitumor effect of ECyd would be enhanced by encapsulation into long-circulating liposomes and prolonged exposure of tumor cells to ECyd above C_{min}. PEGylated liposomes containing ECyd were then prepared. The encapsulation ratio was 5%. Liposomal ECyd was administered as free ECyd to tumor-bearing BALB/c mice on days 5 and 10 (double administration) or on day 8 (single administration). Unexpectedly, however, liposomal ECyd inhibited tumor growth less efficiently than unencapsulated ECyd, irrespective of the injection schedule (Table 1- 1, Experiment 2).

1.1.3.6 PK–PD modeling of liposomal ECyd

To determine the reason why the liposomal ECyd was unexpectedly less effective than free ECyd, the PK of liposomal ECyd was analyzed. Both the liposome membrane and ECyd were traced after administration. As shown in Figure 1- 3C, ~10% of liposomes modified with PEG were present in blood after 24 hr, showing the nature of long-circulating liposomes. Nearly 10% of the injected liposomes reached tumor tissue at 24 hr (Figure 1- 3D). The disposition of total ECyd, which includes released and liposomal ECyd, is also shown in Figure 1- 3C and D. The amounts of total ECyd in blood and tumor were not identical to those of liposomes, indicating the release of ECyd from liposomes. I had hypothesized that ECyd released in and near the tumor would accumulate in the tumor. However, the amount of ECyd was half that of the liposomes in

the tissue. As described above, the liposomal ECyd injection was less effective than free ECyd injection (Table 1- 1, Experiments 1 and 2). Taken together, these results suggest that the free ECyd concentration in the tumor was lower for the liposomal ECyd injection than for the free ECyd injection.

A PK model containing liposomal and free ECyd (Scheme 1A) was then constructed, and curve-fitting was carried out based on this model and the actual data. First, the data on $[^3H]$ CHE-liposome, which correspond to the disposition of the liposome itself, were analyzed according to the two-compartment model consisting of blood and tumor compartments, since the change in disposition of the liposomes could be approximated by elimination by reticuloendothelial system and distribution in the tumor. Data on $[^3H]$ ECyd were analyzed using the three-compartment model. Based on the PK parameters determined by the simulations, latency (encapsulation efficiency *in vivo*) were calculated (Figure 1- 5). The latency curve was a combination of two functions that appear to reflect fast and slow releases of ECyd from liposomes. These two release rates might be due to the presence of multilamellar and unilamellar vesicles. The release rate constant ($k_{rel,tumor}$) was calculated to be 0.02 hr^{-1}, a three-fold higher value than the rate constant of the slow release in blood ($k_{rel,blood,slow}$) (Table 1- 2 and Figure 1- 2A). Effective times for which tumor cells were exposed to free ECyd above the C_{min} value (61.1 fmol/g) obtained from the free ECyd injection data and the simulation were calculated (Figure 1- 3A and B, and Figure 1- 4B). The IR data from the single injections of the liposomal ECyd were on/near the effective time–IR curve (Figure 1- 4C, circles). In contrast, data from the double injections of the liposomal ECyd were out of the curve (triangles). It has been reported that second injections of PEG-liposomes are cleared rapidly from blood (accelerated blood clearance (ABC) phenomenon) [18-21]. The actual effective times for double administration might be half of those in the simulation, owing

to the ABC phenomenon of the second injection of liposomes. The insufficient antitumor activity and the simulation suggest that the PEG-liposomes did not deliver free ECyd to the tumor more efficiently than the free ECyd injection. These results indicate that the availability of “free” ECyd in the tumor tissue is important.

1.1.3.7 Enzymatic synthesis of the phospholipid derivatives of ECyd

The simulations based on the PK data of free and liposomal ECyd prompted the use of ECyd-phospholipid derivatives that may improve delivery to the tumor and availability in the tumor. Three ECyd-phospholipid derivatives were prepared, in which phospholipids were attached to ECyd via the 5'-phosphate (Figure 1- 1). The ECyd-phospholipid derivatives have affinity to the cell membrane, and might move from liposomes to the cell membrane. The derivatives on the inner membrane might release the monophosphate derivative of ECyd (ECMP) into the cytosol of tumor cells. This might overcome the important barriers of uptake by transporter(s) and 5'-phosphorylation by UCK2. Controlled release of ECMP from the phospholipid derivatives might be useful, since the first phosphorylation of nucleoside analogs is a determining factor for their efficacy[22].

An enzymatic method was previously developed for the preparation of phospholipid derivatives of nucleosides from a nucleoside and a phosphatidylcholine by a one-step reaction, in which phospholipase D-catalyzed transphosphatidylation, namely, the regiospecific transfer reaction of the phosphatidyl residue from a phosphatidyalcholine to the 5'-hydroxyl of a nucleoside, was used [23]. The phospholipid derivatives of ECyd used in this study were effectively synthesized by this method.

1.1.3.8 The improved antitumor effects of liposomes containing ECyd-phospholipid derivative

Liposomes containing ECyd-phospholipid were administered to tumor-bearing mice. As shown in Table 1- 1 (Experiment 3), liposomal DPPECyd inhibited tumor growth by 55% while free ECyd inhibited it by 35%. In addition, DPPECyd did not cause body weight

change, an indicator of side effects. Liposomal DSPECyd was most effective and inhibited tumor growth by 68%, although it caused a decrease in body weight, suggesting severe side effects. In contrast, liposomal DOPECyd showed tumor growth inhibition similar to that by free ECyd. These results indicate that ECyd-phospholipid derivatives could enhance the antitumor activity of ECyd by increasing its availability in tumor tissue.

1.1.4 Discussion

The antitumor effect of ECyd was AUC-dependent *in vitro* and time-dependent *in vivo* (Table 1- 3 and Table 1- 1, Experiment 1). It appears that the efficacy of ECyd actually depends on both concentration and time, and that apparent dependency changes with the experimental conditions. ECyd is taken up into cells by transporters [24] and phosphorylated by UCK2 to ECMP[13,14]. The actual drug, ECTP, is formed by subsequent phosphorylation reactions from ECMP, but the first phosphorylation reaction would be most important for the efficacy of ECyd. The incorporated ECyd is excreted from cells by transporter(s). When measured *in vitro*, the influx clearance of ECyd was lower than its efflux clearance, suggesting the presence of efflux transporter(s) (data not shown). However, it is possible that the phosphorylated forms of ECyd are hardly excreted. The conversion of ECyd to ECMP by UCK2 would not occur substantially at low extracellular ECyd concentrations because of the efflux transporter(s). Thus, an amount of ECyd higher than a certain "threshold" would be required for the cytotoxic effect, and totally synthesized ECTP should be dependent on both its extracellular ECyd concentration and exposure time. This could be a reason for the AUC-dependency of ECyd *in vitro* (Table 1- 3). Considering that the uptake of ECyd and its conversion to ECMP are carried out by enzymes, saturation of their activities can be easily assumed. A highly excessive amount of ECyd

would not lead to dose-dependent accumulation of ECTP. Therefore, dose-dependency of the efficacy would be present within a certain concentration range. *In vitro*, extracellular ECyd concentration is thought to be constant during the exposure time, due to a lack of clearance from the medium. On the other hand, the half-life of ECyd in blood was very short, and ECyd concentration in the tumors varied, increasing and then decreasing (Figure 1- 3A and B). Tumor cells near blood vessels, in particular, would be exposed transiently to a high concentration of ECyd. In this study, a putative concentration value, C_{min}, was proposed in the simulation to explain the schedule-dependency of the ECyd antitumor effect *in vivo*. The calculated effective time based on this value could explain the efficacy of free and liposomal ECyd (Figure 1- 4B and C). Since the uptake, excretion, and phosphorylation of ECyd are conducted by enzymes, as described above, a simple linear correlation between AUC and IR would not be present. In such cases, the concept of C_{min} might be a good parameter to explain the efficacy of other drugs.

Calculation of release rates of ECyd from PEG-liposomes showed the presence of two values (Table 1- 2 and Figure 1- 5). The $k_{rel,blood,fast}$ and $k_{rel,blood,slow}$ values were calculated to be 0.52 and 0.006 hr^{-1}, respectively. These two release rates could be attributed to the possible presence of two fractions of liposomes, multilamellar and unilamellar vesicles.

The fast rates would reflect ECyd release from the outermost aqueous phase. The release rate constant in tumor tissue ($k_{rel,tumor}$) was calculated to be a three-fold higher value of the rate constant of the slow release in blood ($k_{rel,blood,slow}$). This suggests that certain collapse mechanism(s) of liposomes, such as phagocytization by macrophages, are present near the tumor. Different drug release rates in blood and tumor are suggested in this study, although the same release rates were hypothesized in previous studies by Harashima et al[15,16].

Single and double administration of ECyd encapsulated in PEG-liposomes was less effective than injection of ECyd alone (Table 1- 1 , Experiments 1 and 2). PK analyses indicate that the apparent ECyd concentration in tumor was higher for liposomal ECyd than for ECyd alone (Figure 1- 3B and D). However, the simulation based on the model shown in Scheme 1A suggests that ~75% of ECyd was present in the encapsulated form in tumor tissue (data not shown). This would result in the reduction of the availability of ECyd in the tumor for liposomal ECyd. Thus, it should be emphasized that disposition in a target site, but not in blood, is important for the design of the optimal carrier of a drug.

The simulations based on the PK data of free and liposomal ECyd prompted the use of ECyd-phospholipid derivatives for improvement of the trafficking to and availability in the tumor tissue. Indeed, the liposomes containing DPPECyd and DSPECyd showed increased antitumor effects compared with free ECyd (Table 1- 1, Experiment 3). In contrast, liposomal DOPECyd showed tumor growth inhibition similar to that by free ECyd. Thus, alteration in chain-length might make controlled release possible. The order of IR was DSP > DPP > DOP. This order agrees with that of instability of phospholipids in liposomes. The absence of the unsaturated C–C bond and the short carbon chain destabilizes liposomes and consequently leads to the release of the ECyd-phospholipids and transfer to the plasma membrane of tumor cells. DSPECyd could stay in liposomes, and the controlled release of this ECyd derivative could produce the actual drug ECTP most effectively. Additionally, liposomal DSPECyd caused a decrease in body weight, suggesting side effects, although liposomal DPPECyd and DOPECyd did not. The alteration in chain-length could also control toxicity. The other advantages of the encapsulation of phospholipid-derivatives of ECyd were improved encapsulation ratio (from 5% for ECyd to 100% for the derivatives) and alteration in incorporation pathways, avoiding influx transporters.

In this study, dispositions of free and liposomal ECyd were compared *in vivo*, and the establishment of C_{min} value and resulting effective time in simulation could explain the efficacy of ECyd drugs. It is probable that the effects of type II antitumor drugs that depend on exposure time and the cell cycle can be predicted by simple modeling and calculation using this C_{min} value. An important conclusion is that the encapsulation of ECyd-phospholipid derivatives into long-circulating liposomes could enhance antitumor activity, possibly due to improved availability in the target tissue.

1.1.5 Figures

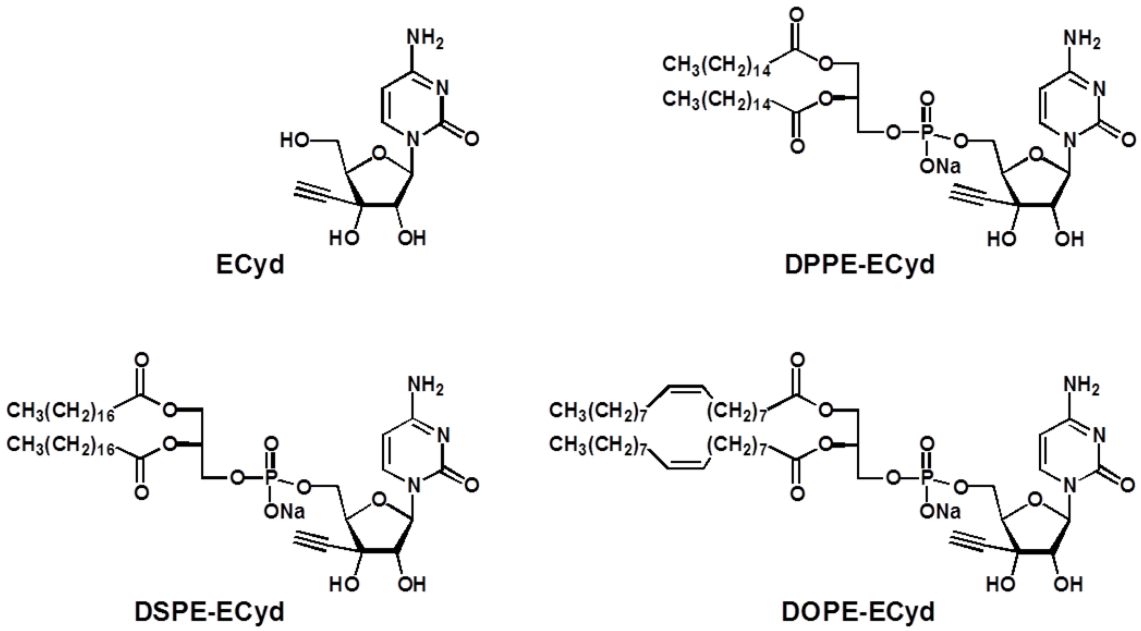

Figure 1- 1 Chemical structures of ECyd and its phospholipid derivatives

A)

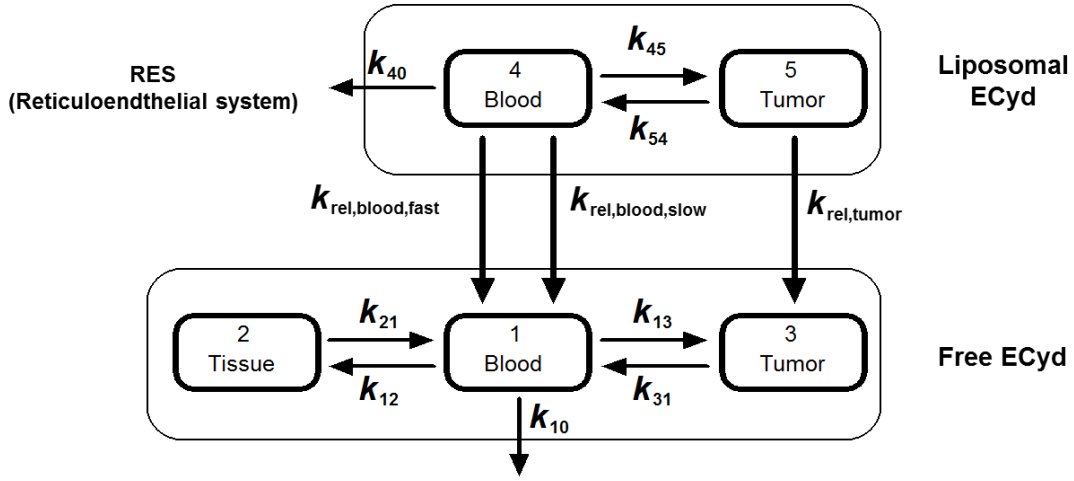

B)

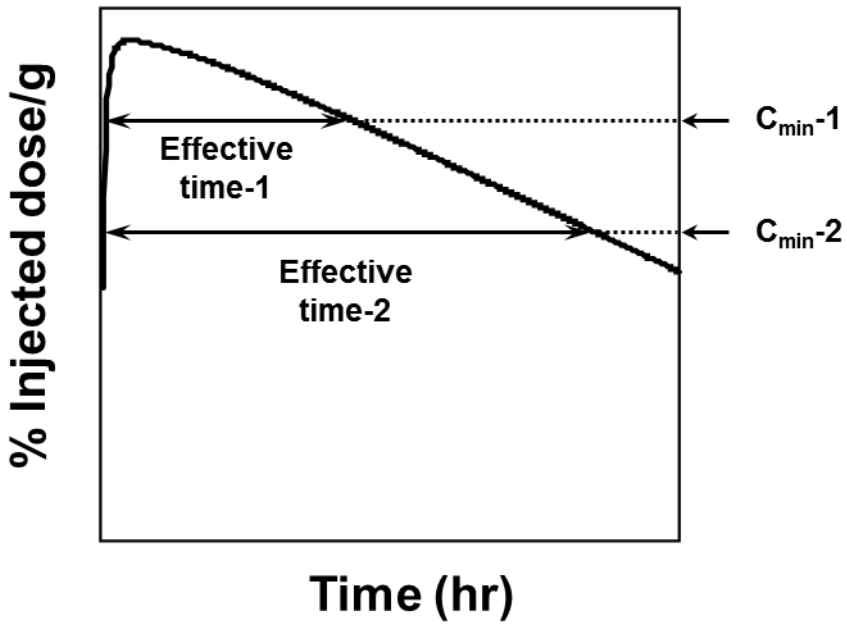

Figure 1- 2 Pharmacokinetic model of ECyd and scheme of description of C_{min} and effective time

A) PK model of free and liposomal ECyd, B) Explanatory drawing of C_{min} and effective time

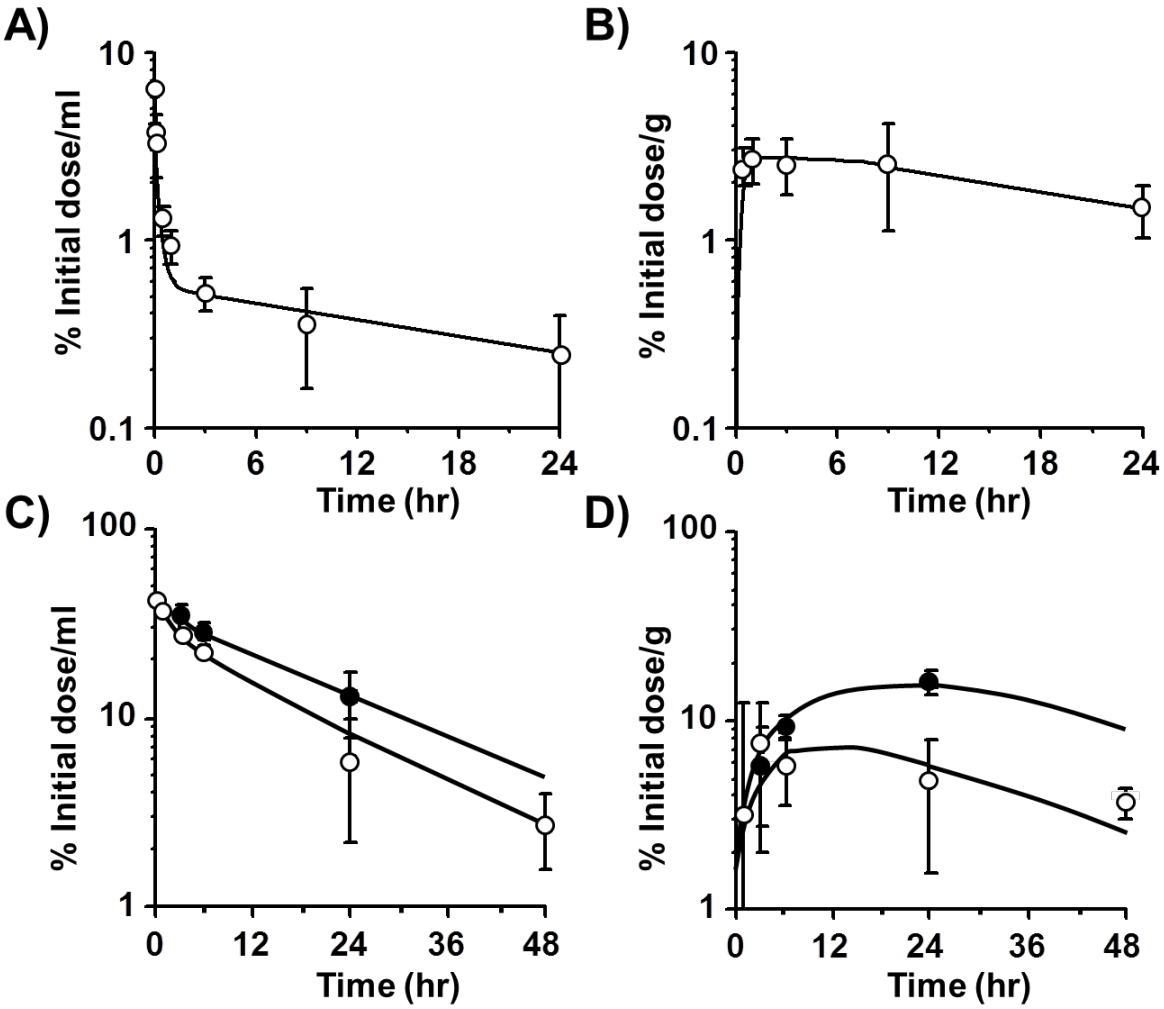

Figure 1- 3 Concentration-time profile of ECyd and liposome

A and B) Concentration of ECyd in blood (A) and tumor (B) upon injection of free ECyd,
C and D) Concentrations of ECyd (open circles) and liposomes (closed circles) in blood (C) and tumor (D) upon injection of liposomal ECyd. The curves are drawn by the simulations based on the PK model shown in Figure 1- 2(B). Bars represent SD.

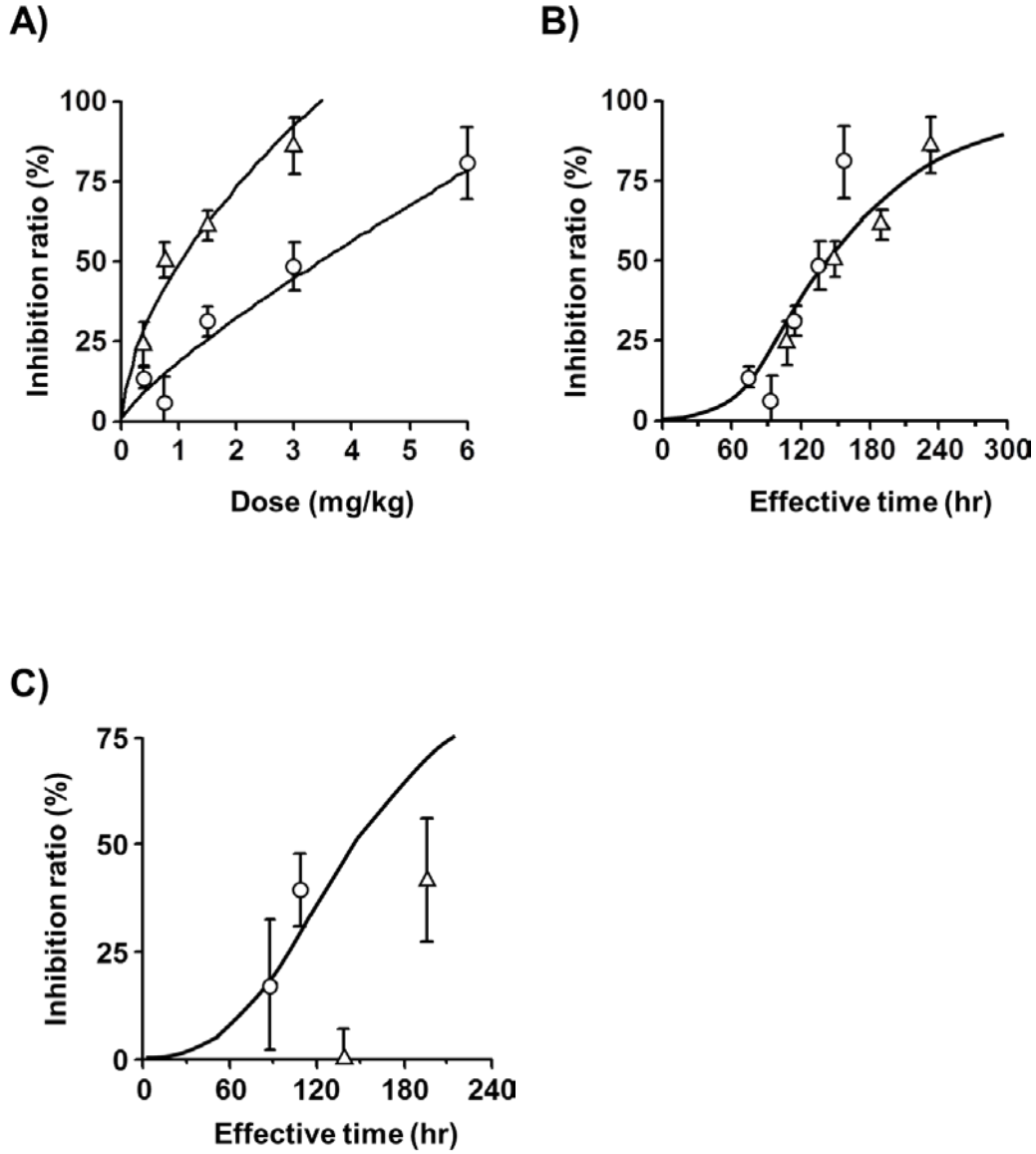

Figure 1- 4 Relationships between administration dose / effective time and IR

(A and B) Relationships between administration dose and IR (A) and between effective time and IR (B) upon injection of free ECyd. (C) Relationship between effective time and IR upon administration of liposomal ECyd. (A) The data shown in Table 1- 1 (Experiment 1) are plotted. (B) The effective time was calculated when the C_{min} value was set as 61.1 fmol/g. The data shown in panel A are replotted using the effective time as the horizontal axis. (C) The data shown in Table 1- 1 (Experiment 2) are plotted using the effective time calculated when the C_{min} value was set as 61.1 fmol/g as the horizontal axis. Circles and triangles represent the data obtained from the single and double injections, respectively. Bars represent SD. The fitted curves in panel A were drawn, using the following equation (eq. 10) IR $=E_{max} \times D^r/(D_{50}^r + D^r)$ where E_{max}, D, and D_{50} represent the maximum efficacy (set as 100%), dose, and 50% inhibitory dose, respectively. The fitted curve in panel B was drawn according to equation 9 in the text, and the same curve was imposed in panel C to show that the IR data of the liposomal ECyd were on/near the effective time–IR curve only for the single injections.

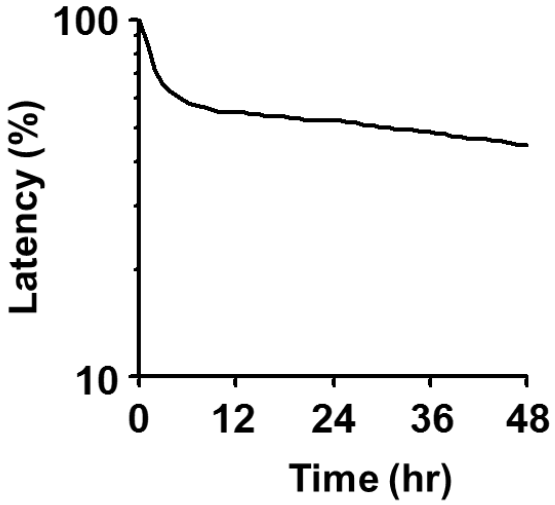

Figure 1- 5 Latency calculated based on the data shown in Figure 1- 3(C)

1.1.6 Tables

Table 1- 1 Inhibition of tumor growth by administration of ECyd and its derivatives

Drug	Dose [a] (mg/kg)	No. of death	BWC (%) [b] on day 15	IR (%) [c] on day 15
Experiment1				
None	0.00	0/4	-2.0	NA [d]
ECyd i.v. on day 8	0.38	0/4	1.3	13.5
	0.75	0/4	15.0	5.9
	1.50	0/4	12.9	31.1
	3.00	0/4	7.3	48.2
	6.00	0/4	10.4	80.7
ECyd i.v. on days 5 & 10	0.19 X 2	0/4	5.2	24.1
	0.38 X 2	0/4	10.0	50.4
	0.75 X 2	0/4	7.9	61.2
	1.50 X 2	0/4	13.6	85.9
Experiment2				
None	0.00	0/4	8.4	NA [d]
Liposome	0.00	0/4	9.4	NA [d]
Liposomal ECyd i.v. on day 8	1.50	0/4	8.9	17.2
	3.00	0/4	8.5	39.5
Liposomal ECyd i.v. on days 5 & 10	0.75 X 2	0/4	8.9	-1.0
	1.50 X 2	0/4	8.5	41.5
Experiment3				
None	0.00	0/5	-15.1	NA [d]
ECyd i.v. on day 8	3.00	0/5	-2.5	35.0
Liposomal DPPECyd i.v. on day 8	3.00	0/5	-2.7	55.2
Liposomal DSPECyd i.v. on day 8	3.00	0/5	-20.9	68.2
Liposomal DOPECyd i.v. on day 8	3.00	0/5	-2.2	32.4

a) As ECyd.

b) Body weight change was calculated according to the following formula:

BWC (%) = [(body weight on day 15) – (body weight on day 0)] / (body weight on day 0) × 100

c) IR on the basis of tumor volume was calculated according to the following formula:

IR (%) = [1−(mean tumor volume of treated group)/ (mean tumor volume of control group)] ×100

d) Not applicable

Table 1- 2 Pharmacokinetic parameters obtained by simulations

PK parameter for Free ECyd	
V_{Ecyd} (mL)	16.9
k_{10} (hr^{-1})	0.34
k_{12} (hr^{-1})	3.23
k_{21} (hr^{-1})	0.39
k_{13} (hr^{-1})	0.02
k_{31} (hr^{-1})	0.33
PK parameters for liposomes	
$V_{liposome}$ (mL)	2.14
k_{40} (hr^{-1})	0.04
k_{45} (hr^{-1})	0.003
k_{54} (hr^{-1})	0.06
PK parameters for liposomal ECyd	
$k_{rel,blood,fast}$(hr^{-1})	0.52
$k_{rel,blood,slow}$(hr^{-1})	0.006
$k_{rel,tumor}$(hr^{-1})	0.02

Table 1- 3 Relationship between exposure time and IC_{50} *in vitro*

Exposure time (hr)	IC_{50} (nM)	AUC (nM.hr)
4	6.7×10^2	2.7×10^3
12	3.0×10^2	3.6×10^3
24	0.8×10^2	1.9×10^3
48	0.7×10^2	3.4×10^3

AUC=exposure time $\times$ IC_{50}

2 CHAPTER2

2.1 Statistical analysis of Amenamevir (ASP2151) between pharmacokinetics and clinical efficacies with non-linear effect model for the treatment of Genital Herpes

(Original article was published in Clinical Pharmacology in Drug Development 3(5) 365-370)

2.1.1 Introduction

Recurrence of genital herpes is usually caused by herpes simplex virus type 2 (HSV-2) and less commonly by herpes simplex virus type 1 (HSV-1) [25]. Almost 50 million American adults and adolescents (20%) are infected with genital herpes: it is one of the most common sexually transmitted diseases[26]. HSV-2 and HSV-1 are neurotropic pathogens, establishing latency within the sensory ganglia after primary infection and reactivating by traveling from the nervous system to the skin and mucous membranes to result in recurrent infection. The recurrence of genital symptoms is very typical, with up to 80% of HSV-2-infected patients experiencing recurrent outbreaks within the first 12 months following the first episode. It is often the first episode that exhibits the most severe lesions and residual symptoms, because the immune system is naive to the infection. It should be noted that the subsequent recurrences are also painful and interfere with daily life, thereby reducing patient quality of life (QOL)[25-27]. Amenamevir which is an oxadiazolylphenyl derivative[28] is the international non-proprietary name for ASP2151. It is synthesized by Astellas Pharma Inc. It is a structurally novel class of helicase-primase inhibitor and demonstrated more potency *in vitro* anti-viral activity with low cytotoxicity against varicella-zoster virus (VZV), HSV-1, and HSV-2 than acyclovir

(ACV). The *in vivo* anti-viral activity of Amenamevir significantly reduced the mortality and the cumulative disease score in the HSV-infected animal model in mice[29].

Phase II randomized trial assessed the safety and efficacy of Amenamevir for episodic therapy of recurrent genital herpes was conducted[30]. Valacyclovir (VACV) was used as a comparator because acyclovir (ACV) now increasingly replaced by its prodrug VACV in genital herpes treatment[31].

Participants self-initiated with Amenamevir (100, 200, or 400 mg daily for 3 days), Amenamevir (1200 mg as a single dose), placebo for 3 days, or VACV (500 mg twice daily for 3 days).

Base on the non-clinical PK/PD analyses, PK/PD parameter T_{100}, which is the length of time the Amenamevir concentration in plasma exceeds 100 ng/ml, the most accurately predicted the efficacy of Amenamevir with respect to the complete inhibition of HSV-1 replication. As the activity of Amenamevir against HSV-2 and VZV is approximately 2-fold lower than that against HSV-1, I speculate that HSV-2 and VZV growth can be completely suppressed using a dosage regimen resulting in a T_{200} of close to 24 h per day. Consequently, the target concentration of Amenamevir in plasma for treating herpes simplex and herpes zoster is estimated to be 200 ng/mL.

Based on the observed concentrations of Amenamevir in plasma in healthy volunteers who participated in a phase I study, the target center dose of Amenamevir for genital herpes (usually caused by HSV-2) was set to 200 mg/patient, which was estimated to give approximately 21 h in terms of T_{200}[32].

Clinical development of Amenamevir is ongoing in Japan. Phase 3 study for genital herpes patients is enrolling process. Amenamevir will be expected to show the good clinical efficacy and safety for the genital herpes patients.

In this report, the population pharmacokinetic (PK) model was developed to characterize the PK of amenamevir in genital herpes patients. Additionally, PK/PD analysis was conducted to consider the PK parameters related to the efficacy endpoints.

2.1.2 Methods

2.1.2.1 Patient population and study design

The details of the original clinical study design have been reported.[30] This was a Phase II, dose-finding, double-blind, double-dummy, randomized, parallel group, active/placebo controlled study comparing the efficacy and safety of four dosing regimens of Amenamevir to VACV and placebo. Subjects who provided written Informed Consent were screened for eligibility to participate in the study based on medical history, physical examination and laboratory testing. Subjects were randomized equally to one of six arms of Amenamevir 100 mg, 200 and 400 mg once-daily dosing for 3 days and Amenamevir 1200 mg once-daily dosing for 1 day, VACV 500 mg twice daily dosing for 3 days, and placebo for 3 days. All study medication was taken p.o. under fed condition. To maintain the double-blind nature of the study, all subjects received study drugs twice daily dosing for 3 days, by receiving matching placebo tablets or capsules. Participants were to self-initiate treatment after experiencing the first sign or symptom of recurrence, in line with previously published trials with similar methodology[33].

The analysis dataset consisted of those patients who received at least one dose of Amenamevir and who had at least one drug concentration for a time point after dosing. Total 273 patients were used to the analysis. The study protocol and informed consent forms were reviewed by an institutional review board (IRB) for each study site. IRB list is shown on the online supplement because of space consideration. A signed informed consent form was obtained from each patient before the initiation of any study-specific

procedure. The study was conducted in accordance with the ethical principles stated in the Declaration of Helsinki, Good Clinical Practice, International Conference on Harmonization guidelines, and applicable laws and regulations.

2.1.2.2 PK sampling

Blood samples for measurement of amenamevir were collected at screening and at the clinical visits through Day 1 to 4 once a day. Unchanged plasma amenamevir concentrations were measured using a validated liquid chromatography-tandem mass spectrometry (LC-MS/MS) method based on Food and Drug Administration (FDA) validation guidance at Covance Laboratories, Ltd. Amenamevir was isolated from plasma by liquid-liquid extraction using tert-butyl methyl ether. Deuterium-labeled Amenamevir was used as the internal standard. The extracts were analyzed by LC/MS/MS, using isocratic elution, with 40% of 0.1% formic acid in water and 60% 0.1% formic acid in methanol, on a Chromolith, SpeedROD, RP-18e, 50 x 4.6 mm column, using Sciex API 4000 with a turbo ion spray interface in positive ion mode. The method was validated over a range of 5‑5000 ng/mL. Intra- and inter-precision (coefficient of variation, CV) values were from 4.2% to 8.3%. Intra- and inter--assay accuracy (residual, RES) values were from 101.1% to 104.0% for these same QCs. The limit of quantification for Amenamevir was 5 ng/mL using 0.1 mL plasma.

2.1.2.3 Clinical Efficacy

2.1.2.3.1 Time to lesion healing

Time to healing of all lesions was determined by the Investigator (time from therapy initiation to re-epithelialization of all lesions, excluding aborted lesions). Time was measured in hours. Aborted lesions were defined as the presence of prodromal symptoms including pain, tingling, itching, and burning, but failure to develop lesions beyond the

macule/papule stage to the vesicular/ulcerative stage. Healed lesions were defined as the absence of crusts, depressions, erosions or ulcerations. Residual erythema in absence of the preceding is defined as healed.

Existing symptom lesions was classified by the site clinician as: macule/papule, vesicle/ pustule/ulcer, crust, or healed lesion. Classification was carried out during the genital examinations on Days 1-6 and on Days 8 and 10 only if lesions had not healed by Day 6 and Day 8, respectively. If the subject had existing symptom lesions at the Day 17 visit, an additional genital exam for lesion classification was performed.

2.1.2.3.2 Duration of viral shedding

Time was measured in hours from initiation of treatment to the first negative viral culture with all negative subsequent cultures for HSV. Swabs of the genital symptomatic area were collected on each subject. HSV viral shedding analysis was measured using the viral culture. Swabs were to be obtained twice daily for culture. Self-swabs by the subject of the genital symptomatic area were collected approximately 12 hours apart from clinic visit swabs. After the first clinic visit, self-swabs were to follow the dosing schedule. If the clinic visit was scheduled in the morning, the subject was to self-swab at the previous evening dose of medication. If the clinic visit was scheduled in the afternoon or evening, the subject was to self-swab with the same morning dose.

2.1.2.4 Population pharmacokinetic modeling

The population PK analysis was performed using the non-linear mixed effects modeling approach[34]. The PPK analysis was performed using NONMEM Version VI Level 1.0 (Icon Development Solutions, Ellicott City, MD) with the software package Pdx-pop (Version 3, Icon Development Solutions, Ellicott City, MD)[35]. The objective function was calculated using first-order conditional estimation with interaction (FOCE-INTERACTION)[36]. Concentration values below the lower limit of quantitation (BLQ)

were excluded from PPK analysis. All tentative covariates were tested in a step-wise addition method at the p=0.05 level of significance to reach the full model. All selected tentative covariates were to be tested in a step-wise backward deletion method at the p=0.001 level of significance to reach the final model. The following covariates were used in the PK parameter-covariate investigation: age, race, sex, food intake time, Height (Ht), weight (WGT), white blood cell (WBC), red blood cell (RBC), hemoglobin (HGB), hematocrit (HCT), platelet (PLT), reticulocyte counts (Ret), Creatinine (Cr), blood urea nitrogen (BUN), albumin (ALB), total bilirubin (BILI), aspartate transaminase (AST), alanine aminotransferase (ALT), alkaline phosphatase (ALP), total protein(TP), and cholesterol (CHO).

A visual predictive check[37] was performed using the final model for the model validation.

2.1.2.5 PK/PD analysis

Individual cumulative T_{200} for three days ($T_{200,day3}$) and T_{200} in the steady states ($T_{200,ss}$) were predicted by the simulation which assumed the 3days dosing or steady state based on the PK parameters from the final model.

Individual $T_{200,day3}$ was summarized into 5 categories by a percentile method, 0%-20%, 20%-40%, 40%-60%, 60%-80% and 80%-100%. Individual $T_{200,ss}$ was summarized into 2 categories by the threshold levels, 15 ,18 and 21 (hrs). Threshold 21hrs was defined based on the phase1 estimation[32], 15 and 18hrs were added to consider the other criteria.

PK/PD analysis was conducted to consider the relationship among categorized $T_{200,day3}$, $T_{200,ss}$ and clinical efficacies which were time to lesion healing and viral shedding.

Hazard ratios compared with placebo based on the proportional hazards model which included gender and number of recurrences in the 12 months prior to randomization were calculated by the categorized $T_{200,day3}$ and $T_{200,ss}$.

2.1.3 Results

2.1.3.1 Demographics

PPK analysis dataset consisted of 273 subjects and 957 plasma drug concentration time points. 78 of the patients were male and 195 were female.

2.1.3.2 Model building

A 1-compartment model in which the inter-subject variabilities with exponential error model with absorption phase was selected to the base model (Table 2-1- 1). Occasional low absorption rate was observed based on the visual inspection of individual time-concentration profiles, therefore K_a and Ka_{low} were estimated separately. Ka_{low} was estimated at the low concentration point defined by the conditional weighted residuals (CWRES) criteria (CWRES>4 on the base model). Bioavailability of each dosage was estimated separately because of non-linear pharmacokinetics found in Phase 1 studies and the low solubility of amenamevir. WGT and ALB were selected to the covariates of the final model (Table 2-1- 1). The population mean CL (L/h), V (L), Ka (h^{-1}), F_{200mg}, F_{400mg} and F_{1200mg} were estimated to be 13.8 (L/h), 143(L), 0.874 (h^{-1}), 0.982, 0.874 and 0.706, respectively. F_{100mg} was fixed as 1. Ka_{low} (h-1) was estimated and its value was 0.00107 (h^{-1}) (Table 2-1- 1). Inter-individual variabilities (CV%) of η_1 and η_2 were estimated to be 19.2 % and 108%, respectively. %RSE of η_1 and η_2 were 14.7% and 20.6%, respectively. Residual sum of squares (CV%) was 31.9%. %RSE was 11.6% (Table 2-1- 1). A visual predictive check was done using the final model. The final model provided a good description of the amenamevir concentration-time profiles for 4-dose groups (Figure 2-1-1).

2.1.3.3 PK/PD analysis

Individual $T_{200,ss}$ and $T_{200,3days}$ were simulated by the individual post-hoc parameters and categorized by the method previously described.

For time to lesion healing, no clear trend was found with the categorized cumulative $T_{200,day3}$ (Figure 2-1- 2) , on the other hand, clear trend was found with the categorized $T_{200,ss}$ (Figure 2-1- 3).

For duration of viral shedding, a clear trend was found with the categorized $T_{200,day3.}$ The hazard ratio increased with $T_{200,day3}$ increase (Figure 2-1- 2). Moreover the trend that hazard ratio of longer group was higher than shorter group on the categorized $T_{200,ss}$ comparison especially in the 21 hrs threshold. However, the differences of hazard ratio in both comparisons were not statistically significant (Figure 2-1- 3).

2.1.4 Discussion

I present a first population PK modeling analysis of amenamevir. Dose regimens were multiple once-daily dosing for 3 days (100, 200 and 400 mg) and single once-daily dosing (1200 mg). The plasma concentration-time course for amenamevir in patients with genital herpes was accurately described by a 1-compartment model with first order absorption. The PK model parameters were precisely determined. The final PK model retained the effect of WGT and ALB on CL. However, the WGT and ALB effect for CL was small. Mean ± SD of WGT was 79.3 ± 19.7 kg in this study, CL changed from 90% to 114%. Mean ± SD of ALB was 44 ± 3 g/L, CL changed from 96% to 104%. Weight effect might be a small concern when amenamevir is administered to the small body size patients to maintain the efficacy although the effect to T_{200} was small.

Based on the PK/PD analysis using both oral administration and continuous infusion data *in vivo*, the time above 200 ng/mL (T_{200}) for 21-24 hours in one day was considered to be important for amenamevir efficacy [30]. Threshold level estimated *in vivo* study was expected to be obtained by 200 and 400 mg and dosing, however, all dose cohorts were

effective in this clinical study. One possible reason was that clinical dose level and dose selecting rationale were set based on the severe assumption.

A clear trend was found between clinical efficacies and T_{200}. The patients whose $T_{200,ss}$ were above threshold from 15hrs to 21hrs showed the high hazard ratios in both PD parameters (Figure 2-1- 3). Cumulative $T_{200,day3}$ ranges of 20%-40% and 40%-60% categories were 37.77-47.65 hrs and 47.65- 61.00 hrs, 15 hrs/day might be an enough concentration to show the efficacy of amenamevir.

Duration of viral shedding indicated a clear difference than Time to lesion healing. This trend was significantly shown in the categorized $T_{200,ss}$ analyses. One possible explanation was that viral shedding might quantitatively reflects the efficacy of amenamevir. Generally, genital herpes proceeds with viral shedding, amenamevir could suppress the virus replication by keeping the high concentration.

These finding suggested that it could be necessary to maintain the amenamevir concentration above the threshold level to prevent the virus replication. Recent studies have used polymerase chain reaction (PCR) analysis to measure viral shedding in the presence of lesions[38-40] because PCR analysis is a more sensitive test for HSV detection than culture, PCR could not evaluate the living virus, viral shedding was measured using the viral culture and PCR was only used for confirmed diagnosis in this study. While the argument linking HSV shedding to transmission is biologically plausible, there is a paucity of data supporting shedding as a surrogate for transmission[41], Amenamevir leastwise showed the clear suppression of viral replication by maintaining an Amenamevir concentration of at least 200 ng/mL.

2.1.5 Conclusion

An accurate amenamevir PK model for genital herpes patients was developed by using the 1-compartment with first-order absorption. I've found T_{200} was possible correlated with time to lesion healing and viral shedding, consistent with *in vivo* results.

The results indicate that $T_{200,day3}$ and $T_{200,ss}$ probably be related marker to the duration of viral shedding in the genital herpes patients.

2.1.6 Figures

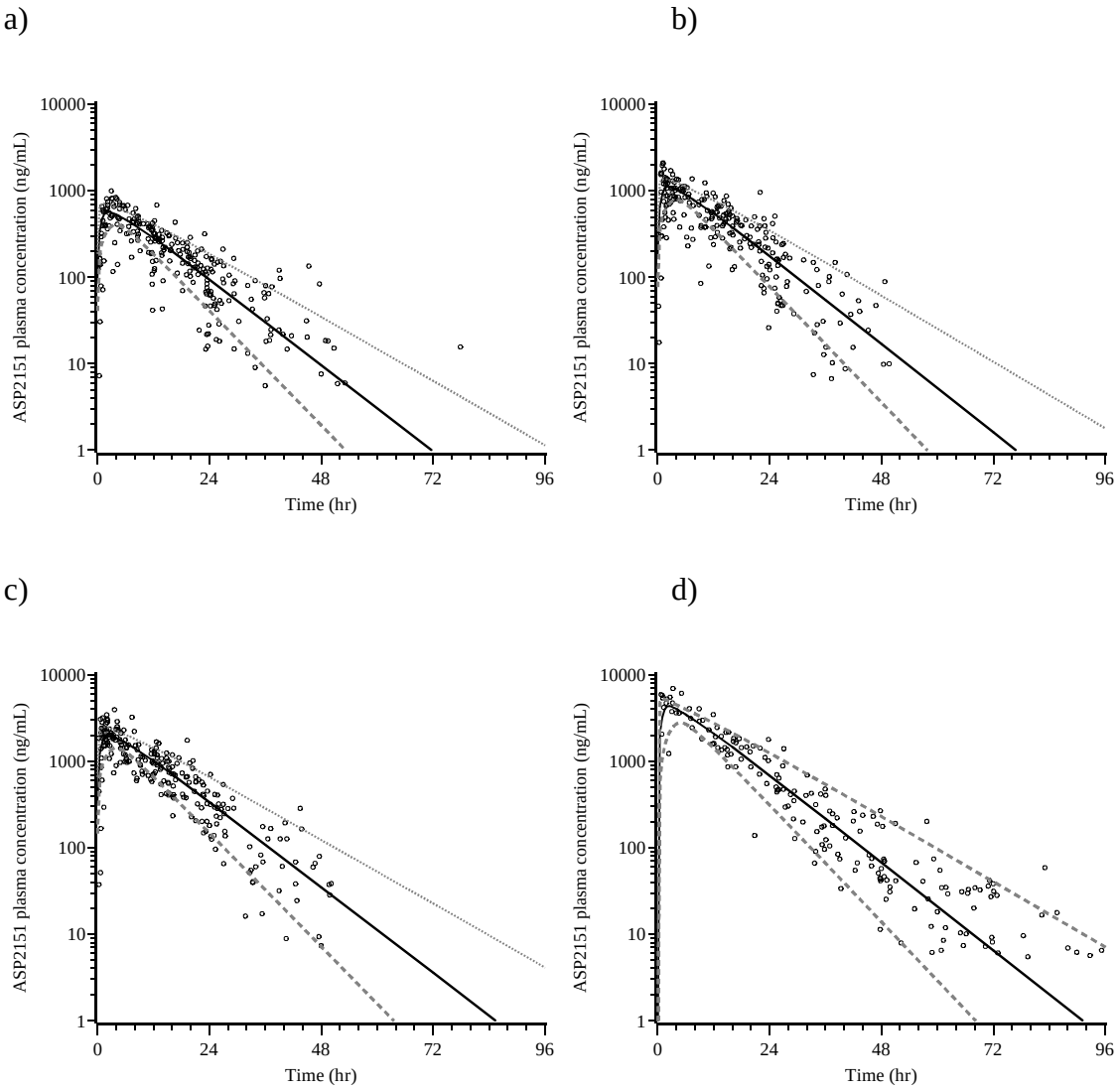

Figure 2-1- 1 Visual predictive check

a) 100mg, b) 200 mg, c) 400 mg, d)1200 mg

Solid line: Median, Dotted line: 90%CI, for 100,200 and 400mg, steady states was assumed to construct the 90%CI.

a)

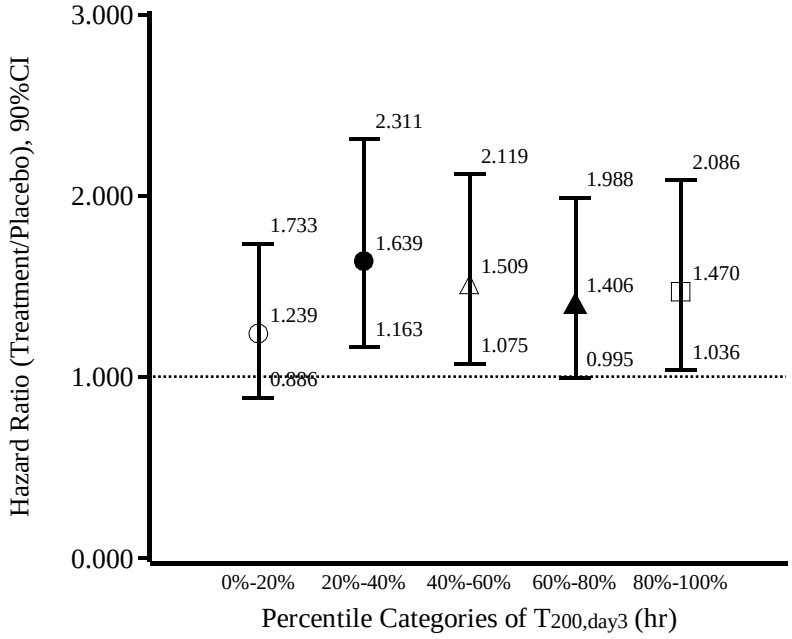

b)

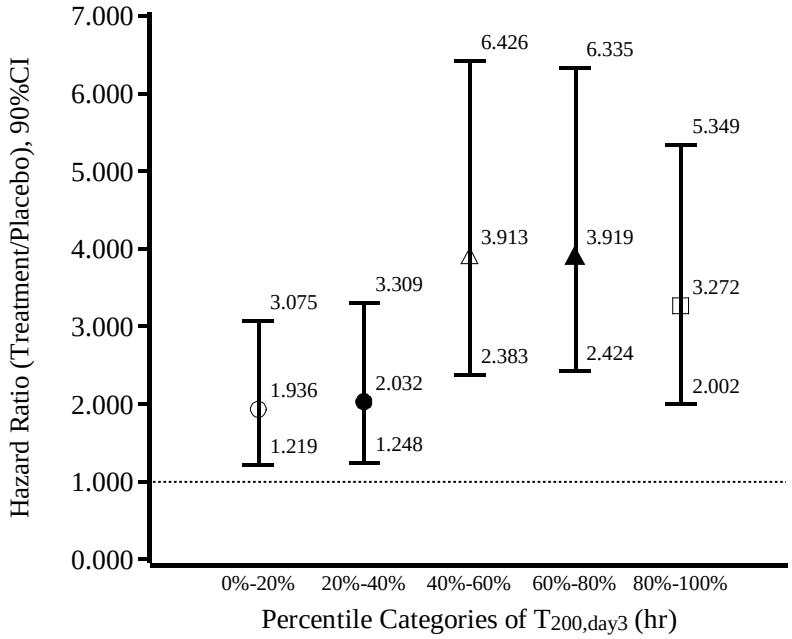

Figure 2-1- 2 Hazard ratio for comparison with placebo by the percentile categories: $T_{200,day3}$

a) Time to lesion healing, b) Duration of viral shedding

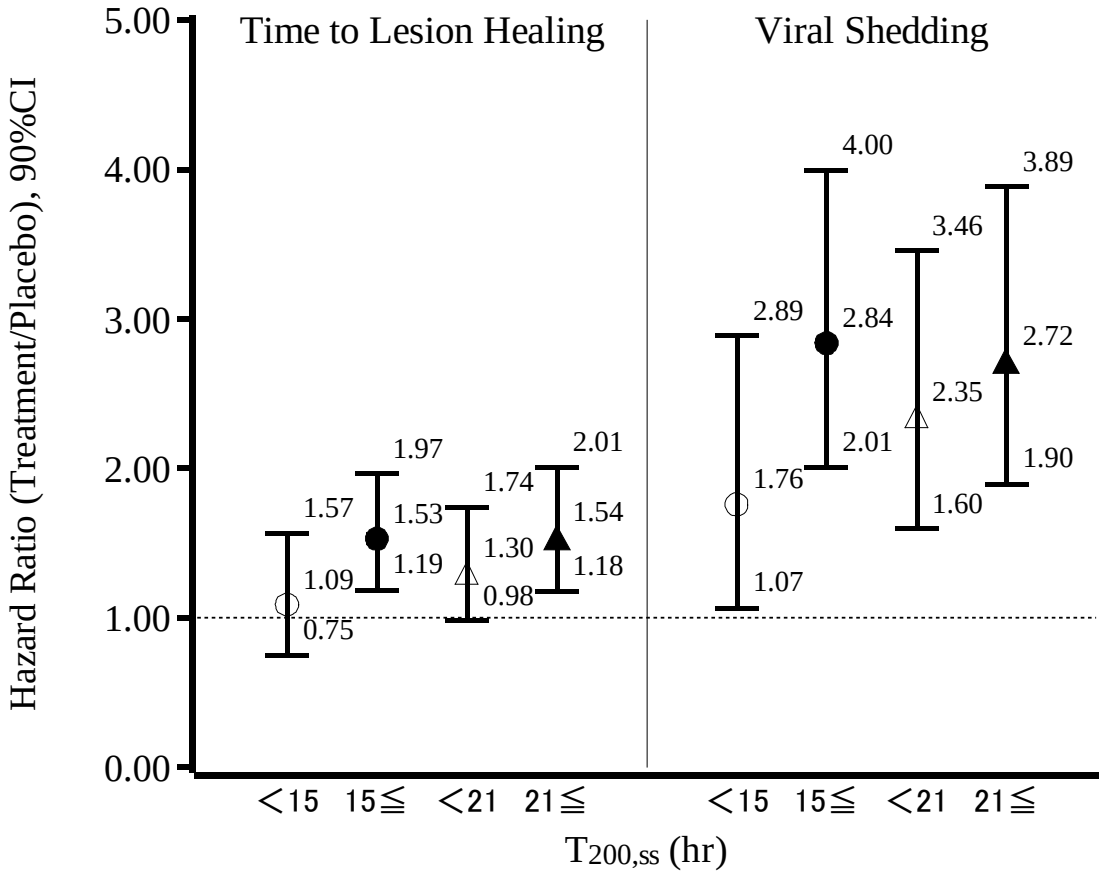

Figure 2-1- 3 Hazard ratio for comparison with placebo by the time categories: $T_{200,ss}$

Result of the 18hrs threshold were not shown because of the same trend as 15hrs and 21hrs

2.1.7 Tables

Table 2-1- 1 Population PK parameters of Base and final model

PK parameters	Final Estimate(%RSE[1])	
	Base model Obj=10220.187	**Final model** Obj=9985.155
CL (L/h)	13.9(4.28%)	13.8(4.28%)
V (L)	143(4.28%)	143(4.31%)
$T_{1/2}$[2] (hr^{-1})	7.1	7.1
Ka (hr^{-1})	1.02(26.50%)	0.874(15.70%)
Ka_{low} (hr^{-1})	0.00182(69.80%)	0.00107(63.30%)
F_{200}	0.977(6.10%)	0.982(6.02%)
F_{400}	0.891(6.04%)	0.874(5.74%)
F_{1200}	0.700(6.46%)	0.706(6.15%)
WGT for CL	-	-0.433(14.00%)
ALB for CL	-	0.561(38.30%)
η_1 for CL	23.8%(11.90%)	19.2%(14.70%)
η_2 for Ka	125%(29.40%)	108%(20.60%)
Err1	31.9%(11.40%)	31.9%(11.60%)

1: %RSE is percent relative standard error (100% x SE/EST)

2: T1/2 = ln2/(CL/V)

Obj: Objective function

2.2 Integrative Pharmacokinetic-Pharmacodynamic Modeling and Simulation of Amenamevir (ASP2151) for Treatment of Recurrent Genital Herpes

2.2.1 Introduction

Recurrence of genital herpes is usually caused by HSV-2 and less commonly by HSV-1 [25]. Almost 50 million American adults and adolescents (20% of the total population) are infected with genital herpes: it is one of the most common sexually transmitted diseases [26]. The recurrence of genital symptoms is very typical, with up to 80% of HSV-2-infected patients experiencing recurrent outbreaks within the first 12 months following the first episode.

Amenamevir is a novel drug that targets the viral helicase-primase complex. This protein complex is essential for herpes simplex virus (HSV) DNA synthesis, making helicase-primase inhibitors such as amenamevir a potential treatment option for genital herpes. A pharmacokinetic / pharmacodynamic (PK/PD) approach for anti-virus drug is similar to the development of antibiotics, and *in vitro* IC_{50} is used to predict the clinical dose *in vivo* animal model [42]. Amenamevir has demonstrated higher potency *in vitro* antiviral activity against HSV-1 and HSV-2 than acyclovir [29].

A phase 2 study (ASP2151 CL-101 study) was performed in the United States to compare the safety and efficacy of four different dose regimens of amenamevir with valacyclovir and placebo in parallel in the acute treatment of recurrent genital HSV infection. At the first sign of recurrence, patients self-initiated treatments with amenamevir 100, 200, or 400 mg daily for 3 days, 1200 mg as a single dose; placebo for 3 days; or valacyclovir 500 mg twice daily for 3 days. Dose and regimen were determined based on those results and PK profile of amenamevir to maintain time above 200 ng/ml of plasma

amenamevir concentration, T_{200} [32]. Of 695 patients randomized to the treatments, data from 437 patients with recurrent infection were analyzed. The primary efficacy endpoint was time to lesion healing which was shorter in all amenamevir groups and the valacyclovir group compared with placebo, but a dose-response relationship was not evident. All groups except amenamevir 100mg showed a higher proportion of aborted lesions compared with placebo[30].

Population PK analysis of amenamevir was conducted to estimate patients' PK profiles using 957 plasma samples in 273 genital herpes subjects in CL-101study. The plasma concentration-time courses for amenamevir were described using a one-compartment model with first-order absorption. Exploratory PK and PD analysis was conducted to find an appropriate PK-related parameter which correlates with PD instead of finding dose-PD relationship, using individual PK parameters derived from the final model by the population analysis. The variable T_{200} was found to correlate with time to lesion healing and viral shedding, which is consistent with the *in vivo* results [43]. However, these correlations were not statistically significant, because T_{200} was dose dependent parameter after all.

In CL-101 study[30], dose-dependent efficacy was not evident in the primary analysis using time to lesion healing, although dose-dependent efficacy had previously been suggested in guinea pigs [28]. To discuss address this inconsistency between clinical and non-clinical results, I conducted additional PK/PD modeling and simulations using the same component model to for both humans and guinea pigs have conducted in the present study with a built-in biomarker—number of virus plaques, which explains the time-dependent antivirus efficacy of amenamevir—to combine the PK of Amenamevir and lesion scores as an efficacy endpoint. Furthermore, non-drug related such as immune response was added to explain the difference.

In general, screening process of new drugs is conducted by using animal to confirm the efficacy, safety and pharmacokinetic. After that, these endpoints are confirmed in clinical trials. Amenamevir showed effective anti-virus action dose-dependently in guinea pigs but not in humans as stated above. To fully understand the phenomenon is somewhat challenging theme, although many drug candidate compounds may have same theme in drug development stage. In this report, I tried to fill a gap between non-clinical and clinical results with the same PK/PD model both animal and human, which is bi-directional translational modeling and simulation approach.

2.2.2 Materials and methods

2.2.2.1 Analysis data from clinical and non-clinical studies

The present study is a population PK/PD analysis using the obtained PK and PD data in the previous clinical and non-clinical studies[28-30]. The scheme of the PK/PD model applied in this study is shown in Figure 2-2- 2. As mentioned in Introduction, the results of the previous virus plaque study provided the possible relationship of viral dynamics with amenamevir concentration[32], and efficacy such as suppression of lesion scores was expected to correlate with amenamevir concentration. The present PK/PD model assumes that the time-dependent increase in number of virus plaques is reduced by amenamevir, and the increase of lesion score is dependent on the virtual number of virus plaques. Data from previous studies were reanalyzed in the present study as follows:

1. Virus plaque assay data were used for constructing virus plaque PD model component.
2. Plasma concentration data of amenamevir in guinea pigs and humans (reference) were used for constructing the PK model component.
3. Lesion score data in guinea pigs and humans were used for logit model analysis.

The experimental conditions for the previous studies will be described briefly in subsequent sections.

2.2.2.2 Antiviral compound and sample measurement

Amenamevir (molecular weight, 482.55; international non-proprietary name, amenamevir) was synthesized by Astellas Pharma Inc. (Tokyo, Japan). Sample measurement was conducted using a validated liquid chromatography-tandem mass spectrometry (LC-MS/MS) method based on FDA validation guidance at Covance Laboratories, Ltd[43]. The lower limit of quantification (LLOQ) of this assay for amenamevir was 5 ng/mL when 0.1 mL plasma was used. The LLOQ data were treated as zero and not used for modeling

2.2.2.3 Viruses and cell lines

HSV strains clinically isolated in the US were kindly provided by Dr. Nancy Sawtell (Cincinnati Children's Hospital Medical Center, Cincinnati, OH, USA). Other viruses and cell lines were provided by Rational Drug Design Laboratories (Fukushima, Japan). Human embryonic fibroblast (HEF) cells and Vero cells were grown in Eagle's minimum essential medium supplemented with 10% fetal bovine serum (FBS), 100 units/mL penicillin G, and 100 μg/mL streptomycin (Invitrogen, Carlsbad, CA, USA). HSV-1 and HSV-2 were propagated using HEF cells in maintenance medium containing 2% FBS.

2.2.2.4 Virus plaque reduction assay

The antiviral activities of amenamevir against HSVs were tested using a plaque reduction assay, as described previously [29,32] to determine the concentration and time dependent effects of amenamevir. Briefly, HEF cells were seeded into multiwell plates and incubated until they formed a monolayer. After the medium was removed, the cells were infected with HSV-1, and the plates were further incubated for 1 h at 37°C. The cells were washed twice with maintenance medium and then treated with the test compound until clear plaques appeared. The cells were then fixed with 10% formalin in phosphate-buffered

saline, stained with a 0.02% crystal violet solution, and the number of plaques was determined under a light microscope. Concentrations of amenamevir were 0.01, 0.03, 0.1, 0.3, 1, 3, 10 and 30 μ M. Duration times of the incubation were 6, 8 and 24 h. These data were included in the present study to simulate the virtual time-course profiles of virus plaques in guinea pigs and humans in combination with their PK data.

2.2.2.5 PK study in guinea pigs

All animal experimental procedures were approved by the Animal Ethical Committee of Yamanouchi Pharmaceutical Co., Ltd. (currently known as Astellas Pharma Inc.). Female Hartley guinea pigs were purchased from Charles River Laboratories (Kanagawa, Japan). Amenamevir at doses of 0.3, 1.0, 3.0 mg/kg were administered as methylcellulose suspension via oral to guinea pig (n = 3 for each group, 4 weeks of age). Plasma samples were obtained at 0.25, 0.5, 1, 2, 4, 8, 12 and 24 h after dosing.

2.2.2.6 PK study in humans

In the present study, the estimated population pharmacokinetic parameters for amenamevir concentration data, which were collected at the time for screening and at the clinical visits once daily through Days 1 to 4 in study CL-101[30], were used.

2.2.2.7 Lesion score measurement in guinea pigs

Antiviral activity of ASP2151 against HSVs in guinea pigs was tested by the evaluation of lesion score as described previously [28]. Briefly, Female guinea pigs (Hartley, aged 4 weeks at the time of viral infection) were intravaginally infected (designated as Day 0 post-infection) with a cotton swab saturated with PBS containing HSV-2 strain G, as described previously [44]. For HSV-2 strain G, the virus pool contained 1.25×10^5 pfU/mL and caused lesions in nearly 100% of control animals. Amenamevir at doses of 0 (placebo), 1, 3, 10, or 30 mg/kg was orally administered twice daily for 5 days starting 3 h after viral inoculation

as a prophylactic treatment, or 4 days after viral inoculation as a therapeutic treatment (n = 10 for each group). The disease profile was monitored daily for 21 days and was scored on a 0-6 composite scale based on the severity of vaginitis and neurological symptoms according to the following criteria:

Score 0: no signs of infection

Score 1: localized, barely perceptible small vesicles

Score 2: small or large vesicles involving 10% to 50% of the area

Score 3: small or large vesicles involving 50% to 100% of the area

Score 4: small ulcers involving 10% to 50% of the area

Score 5: severe ulcers involving 50% to 100% of the area

Score 6: hind limb paralysis or death

The scores of genital herpes in guinea pigs were determined daily. In the PK/PD analysis, the scores on Day 3 were used as the baseline scores to make the modeling easier because of no lesion symptoms until Day 3 after virus allocation. I assumed that disease did not alter the PK of amenamevir.

2.2.2.8 Lesion score measurement in humans

The data for times to healing of all lesions were obtained as the primary efficacy endpoint of Study CL-101 [30]. Genital herpes recurrence was defined as herpes recurrence below the umbilicus and above the knees. Times to healing (h) of all lesions were determined by the study investigator as the times from therapy initiation to re-epithelialization of all lesions, excluding aborted lesions. Aborted lesions were defined by the presence of prodromal symptoms including pain, tingling, itching, and burning, but lesions failed to develop beyond the macule/papule stage to the vesicular/ulcerative stage. Healed lesions were defined as the absence of crusts, depressions, erosions or ulcerations. Residual erythema in absence of the preceding is defined as healed. Existing symptom lesions were classified by the site clinician during the genital examinations on Days 1 - 6,

and also on Days 8 and 10 only if lesions had not healed by Day 6 and Day 8, respectively. If a patient had existing symptom lesions at the visit on Day 17, an additional genital examination for lesion classification was performed. The classification of the existing symptom lesions was categorized in the similar way for guinea pig as follows for a purpose of logit analysis in this study:

Score 0: healed lesion

Score 1: crust

Score 2: vesicle / pustule / ulcer

Score 3: macule / papule

The changes of the scores are unidirectional in the order of 0, 3, 2, 1 and 0. Patients whose scores were maintained to be 0 during the study period were treated as aborted lesions. Mean time course profiles of observed lesion scores are shown in Figure 2-2- 1(a) for guinea pigs and Figure 2-2- 1(b) for humans. The present study was conducted in accordance with the ethical principles stated in the Declaration of Helsinki, Good Clinical Practice, International Conference on Harmonization guidelines, and applicable laws and regulations.

2.2.2.9 Analysis models and simulation data

The analysis conditions in this study are described briefly in this section.

2.2.2.9.1 Population modeling

Logit model analysis was performed via the non-linear mixed effects model [34] using NONMEM Version VI Level 1.0 (Icon Clinical Research, North Wales, PA, USA). Graphical processing of the NONMEM output was performed with SAS Version 8.2, Release 8.02 (SAS Institute Inc., USA). Model selection was based on the goodness-of-fit criteria (log-likelihood difference (l.l.d.) calculated as a difference of objective functions) with visual inspection of the diagnosis plots. A value of l.l.d. more than 3.84 between two

models with a 1 degree of freedom difference was considered to be significant ($p<0.05$). First-order conditional estimation with interaction (FOCE-INTERACTION) [36] was used in NONMEM execution.

2.2.2.9.2 Model validation

Visual predictive check [37] was performed using the final models for guinea pig PK and virus plaque profiles, where 1,000 hypothetical amenamevir concentrations and the numbers of virus plaques were simulated at each time point. The median and 95% prediction interval were constructed from the resulting predictions at each time point. Plots overlaying the medians, prediction interval with observed amenamevir concentrations or observed the numbers of virus plaques were created.

2.2.2.9.3 PK model in guinea pigs

I used a linear single-compartment model with an absorption lag time and first-order absorption as a guinea pig PK model by visual inspection of the observed data. The pharmacokinetic parameters of k_a (absorption rate constant), V/F (apparent distribution volume) and CL/F (apparent total clearance) were defined, where F is the oral bioavailability fraction. Mixed-effect modeling was applied using NONMEM, where log-normal distribution for the inter-individual variability was assumed for each pharmacokinetic parameter, in Equation 1:

$$P_j = \theta_j \cdot \exp(\eta_j) \qquad \text{Eq. 1}$$

where P_j is a parameter of interest in j^{th} subject, θ_j is the population mean of the corresponding parameter, η_j is the random variable which gives the inter-individual variability of P_j from θ_j; η_j was assumed to be normally distributed with a mean 0 and a variance ω^2. Residual error was assumed to be described by a proportional error model given by Equation. 2;

$$Y_{ij} = C_{ij} (1 + \varepsilon_{ij}) \qquad \text{Eq. 2}$$

where Y_{ij} is the i^{th} observed concentration in j^{th} subject, C_{ij} is the predicted concentration by the model, and ε_{ij} was the random variable for residual error which is assumed to be normally distributed with a mean 0 and a variance σ^2.

2.2.2.9.4 PK model in humans

PK model analysis of amenamevir in patients with genital herpes had already been performed using a single-compartment model with first-order absorption[43]. As there were some extremely low concentration data points (LCPs) during the absorption phase in the plasma concentration data, another first-order absorption rate constant ($k_{a,LCP}$) was used in addition to k_a to explain the profile of these LCPs. On NONMEM analysis, the estimated mean (and %RSE) values of apparent clearance (CL/F) was found to be 13.8 (4.28%) L/h, apparent distribution volume (V/F) was 143 (4.31%) L, absorption rate constant (k_a) was 0.874 (15.70%) h^{-1}, and the absorption rate constant for LCP ($k_{a,LCP}$) was 0.00107 (63.30%) h^{-1}. Relative bioavailability (assuming a bioavailability of 1.0 at 100 mg dose) at a dose of 200 mg was 0.982 (6.02%), 400 mg was 0.874 (5.74%), and 1200 mg was 0.706 (6.15%).

2.2.2.9.5 Simulation of PK profiles in guinea pigs and humans

Simulations of plasma amenamevir profiles in guinea pigs and humans were conducted using the population mean PK parameters for guinea pigs and the post-hoc PK parameter estimates for humans to simulate time course profiles of the numbers of virus plaques in those species. The data point treated as LCP were not included in the simulation processes in this study because my modeling method using LCP concept was to explain the outliers (i.e. LCP) and obtain a better estimate for Ka using non-LCP data only. The numbers of LCP data point were 33 in totally 928 points (3.56% total), and I think the effect of omitting the LCP on simulation results is negligible. Time-courses of simulated concentration are shown in Figure 2-2- 5(a) and Figure 2-2- 6(a), and simulation conditions were as follows:

Guinea pig = 0, 1, 3, 10, and 30 mg/kg BID for 5 days;

Human = 0, 100, 200, and 400 mg QD for 3 days or 1200 mg as a single dose.

2.2.2.9.6 PD model for virus plaque

A two-compartment model was applied to explain the concentration and time-dependent changes in the number of virus plaques, as shown in Figure 2-2- 2. A virus cycle was incorporated by defining the amenamevir effective/non-effective compartments, which are connected by first-order rate constants k_{inact} and k_{act} [45]. Increase of virus plaque was assumed as the first-order rate constant (k_{in}), it was fixed to 0.0569 h^{-1} (= ln(60) / 72), which gives the number of virus plaques to be 60 pFU at 72 h based on the study setting. A non-linear drug effect was assumed using the Michaelis-Menten form with maximum drug effect (E_{max}) and a Michaelis constant (EC_{50}).

The mass-balance equations for the number of virus plaques are given as follows.

$$\frac{dV(2)}{dt} = k_{in} \times V(1) - k_{inact} \times V(2) + k_{act} \times V(3) - \frac{E_{max} \times CP}{EC_{50} + CP} \quad \text{Eq. 3}$$

$$\frac{dV(3)}{dt} = k_{inact} \times V(2) - k_{act} \times V(3) \quad \text{Eq. 4}$$

In Eq. 3-4, V(1) represents the number of virus plaques in a hypothetical input compartment, V(2) is the amenamevir effective compartment, V(3) is the amenamevir ineffective compartment; the initial value of V(1) is 60, while those of V(2) and V(3) are 0. Plasma concentration of amenamevir is given by CP. No inter-individual variability was assumed in this case and an additive error model for residual variability was assumed as given in Equation 5;

$$Y_{ij} = C_{ij} + \varepsilon_{ij} \quad \text{Eq. 5}$$

where Y_{ij} and C_{ij} are the observed and model predicted numbers of plaques for the i^{th} sample in j^{th} subject, ε_{ij} is the residual error which is assumed to be normally distributed with a mean 0 and a variance σ^2.

2.2.2.9.7 Simulation of virus plaque profile

Simulations of virtual numbers of virus plaque profiles in guinea pigs and humans were conducted using the simulated amenamevir concentration and the estimated virus kinetic parameters. Simulation settings were as follows.

- Initial administration amount of number of virus plaques was set to 60 pFU
- Time of virus plaque administration was defined as Day 0 (0 h)
- Starting time of amenamevir administration was Day 1 (24 h)

Lesion scores in human on Day 1 were regarded as the initial scores, this is because the Phase 2 study (CL-101) was designed as a self-initiation study, where patients self-initiated treatment and returned to the clinic within 24 h after the initial dose of study drug (Day 1). Time-course of virus plaques is shown in Figure 2-2- 5(b) and Figure 2-2- 6(b).

2.2.2.10 PK/PD Model

2.2.2.10.1 Logit model analysis of lesion score

Logit model analysis was applied to the ordered-categorical lesion score data. Let $Y_{ijk} = Y(t_{ijk})$ be the lesion score at the k^{th} time point t_{ijk}, in the i^{th} individual of the j^{th} treatment group, and Y_{ijk} takes the values of 0, 1, 2, 3, or 4 in the guinea pig study, and 0, 1, 2, or 3 in the human study. The scores 5 and 6 were not included in the analysis for guinea pig because of no observed data for these scores. A logit model for the probability of having a lesion score Y_{ijk} that was equal to or less than a given score y_{ijk} = 0, 1,.., n can be expressed as a cumulative distribution function as follows [46,47].

$$F(y;\theta,\eta) = \Pr\{Y \le y;\theta,\eta\} = \frac{\exp[g(y;\theta,\eta)]}{1+\exp[g(y;\theta,\eta)]} \qquad \text{Eq. 6}$$

where θ is a vector of parameters and η is a random variable. Based on the cumulative probability function, the probability of having a single lesion score was given by Equation 7:

$$\Pr\{Y = y\} = \Pr\{Y \le y\} - \Pr\{Y \le y-1\},$$

where $\Pr\{Y < 0\} = 0$ and $\Pr\{Y \leq n\} = 1$.

The logit, $g(y_{ijk}; \theta, \eta)$ was defined as follows:

$$g(y; \theta, \eta) = \sum_{m=1}^{n} \theta_m \times Q_m(y) + Eff \qquad \text{Eq. 7}$$

for $y_{ijk} = n$, where $Q_m(y_{ijk}) = \begin{cases} 1, y_{ijk} \geq m - 1 \\ 0, \text{otherwise} \end{cases}$.

In guinea pigs, lesion scores increased almost monotonically in the placebo group, however it began to decrease after Day 2 in amenamevir groups and clear dose dependence was observed as shown in Figure 2-2- 1(a). In contrast, lesion scores in humans decreased monotonically over time in both amenamevir and placebo groups, and dose dependence was not clear as shown in Figure 2-2- 1(b). These data suggest that the decrease in lesion scores could not be explained only by the changes of virus plaques reflecting healing of amenamevir (Virus Plaque component) and thus the elapsed time reflecting the healing of the immune response (Time component) was included into the model in this study. For the term of describing drug efficacy (Eff), following model was tested. The term Eff was expressed by the addition of Virus Plaque component and Time component.

$$Eff = \beta_1 \times \text{Virus Plaque} + \beta_2 \times \text{Time} + \eta \qquad \text{Eq. 8}$$

In these models, number of virus plaques (given by 'Virus Plaque') and the elapsed time from virus plaque increase (given by 'Time') were incorporated as fixed effects. This model was built theoretically, no covariates step was conducted. Maximum Likelihood Estimation was used for the fitting and posterior prediction, and individual estimated lesion scores for i^{th} subject at time t (Lesion $score_{i,t}$) were calculated based on the estimated parameters by following equation.

$$\text{Lesion score}_{i,t} = \sum_{m=0}^{n} \Pr_{i,t}\{Y = m \times n, n = 4 \text{ for guinea pig}, n = 3 \text{ for human}\} \qquad \text{Eq. 9}$$

2.2.3 Results

2.2.3.1 PK model in guinea pigs

As shown in Figure 2-2- 3, result of VPC shows that most of the observed values were within 95% prediction interval. Estimated population mean parameters of the PK model for guinea pig PK are summarized in Table 2-2- 1.

2.2.3.2 PD model for virus plaques

Estimated population mean parameters of the PD model for the virus plaque profiles are summarized in Table 2-2- 1. The observed plaque counts versus amenamevir concentration are plotted with the 95% prediction interval in Figure 2-2- 4. The estimated EC_{50} was 127 ng/mL, which is a little smaller than the *in vitro* expected effective concentration of 200 ng/mL [32]. As the result, *in vitro* anti-virus effect of amenamevir was consistent with the virus kinetic model.

2.2.3.3 Logit model for lesion score

Final models for the term logit lesion score in guinea pigs and humans are obtained as follows:

Guinea pig:

$$\text{For Lesion score} =$$

$$0; \text{Logit} = 6.76 + \text{Eff}_{\text{guinea pig}}$$

$$1; \text{Logit} = 6.76 + 3.11 + \text{Eff}_{\text{guinea pig}} = 9.87 + \text{Eff}_{\text{guinea pig}}$$

$$2; \text{Logit} = 6.76 + 3.11 + 4.17 + \text{Eff}_{\text{guinea pig}} = 14.04 + \text{Eff}_{\text{guinea pig}}$$

$$3; \text{Logit} = 6.76 + 3.11 + 4.17 + 5.89 + \text{Eff}_{\text{guinea pig}} = 19.93 + \text{Eff}_{\text{guinea pig}}$$

$$\text{Where } \text{Eff}_{\text{guinea pig}} = -0.265 \times \text{Virus Plaque} - 0.0334 \times \text{Time} \qquad \text{Eq.10}$$

Human:

$$\text{For Lesion score} =$$

$$0; \text{Logit} = -5.21 + \text{Eff}_{\text{human}}$$

$$1;\ \text{Logit} = -5.21 + 1.86 + \text{Eff}_{\text{human}} = -3.35 + \text{Eff}_{\text{human}}$$

$$2;\ \text{Logit} = -5.21 + 1.86 + 3.34 + \text{Eff}_{\text{human}} = -0.01 + \text{Eff}_{\text{human}}$$

$$\text{Where } \text{Eff}_{\text{human}} = -0.0247 \times \text{Virus Plaque} + 0.0424 \times \text{Time} \qquad \text{Eq.11}$$

In these models, a beneficial effect means a decrease of lesion scores while a worsening effect means an increase of lesion scores.

While the fixed effect in Eff of Virus Plaque was negative in both species, the fixed effect in Eff of the Time component by the immune system was negative in guinea pigs but positive in humans. In guinea pigs, both the Virus Plaque and Time components worsened the lesion score. In humans, Virus Plaque worsened the lesion score, whereas immune system improved. Estimated profiles of mean lesion scores were consistent with the observed values in both species (Figure 2-2- 5(c) and Figure 2-2- 6(c)). Some simulations were performed to show the probabilities above each lesion score in guinea pig (Figure 2-2- 5(d)-(g)) and in human (Figure 2-2- 6(d)-(f)), where dose and time dependent profiles are shown. Fitting results are summarized in Table 2-2- 2, and no 95% confidence intervals (CIs) for any fixed effects included 0, indicating that all parameters were significant.

2.2.4 Discussion

In the present study, an empirical PK/PD model, as shown in Figure 2-2- 2 for the helicase-primase inhibitor in genital herpes patients was developed. In this model, the time course profiles of lesion scores was not directly dependent on the amenamevir PK, but it was mainly dependent on the virtual number of virus plaques which suggests a time-dependent anti-virus mechanism of amenamevir.

The PK analysis of amenamevir concentration in guinea pig suggested liner PK profile as shown in Table 2-2- 1 and Figure 2-2- 3. In contrast, the CL/F estimated in the previous study in humans[43] suggested dose-dependent bioavailability as F decreased as dose increased. A possible reason is the difference of the dosage form between the species;

amenamevir was administered in methylcellulose solution to guinea pigs and in tablet form to humans. Amenamevir is poorly soluble, which strongly affects its passive diffusivity (data not shown).

When an allometric scaling [48] was applied, CL/F in humans was estimated about 0.16 L/h/kg, smaller than in guinea pig (2.04 L/h/kg) although the reason of the difference between species was unclear. I focused on the relationship between amenamevir concentrations and virus plaque data in the present study.

I used the virtual number of virus plaques obtained via plaque reduction assay as a marker to explain amenamevir PK/PD mechanism. Goodness of fit of the virus plaque modeling were not enough acceptable especially in the higher concentration range at 6 or 8 hrs exposure. Several models to explain this, i.e. some models including not only the time dependent component but also the dose (concentration) dependent component were tested to try to improve the modeling result, however, no clear improvement was obtained(Data not shown). I could not yet find the reason of this discrepancy at the higher concentration, but I conclude that the current model is sufficient to simulate the efficacy of twice a day or daily dosing of amenamevir because some acceptable result was obtained in the condition of 24hrs exposure which showed the threshold concentration to maintain the amenamevir efficacy throughout the day (Fig.4c). In this analysis, the virus plaque time profile *in vivo* was simulated based on the virus plaque kinetic model, which was built based on *in vitro* data. Several points remain unclear, however—namely the utility of the same viral kinetic model between species, whether or not plasma concentration is the best surrogate marker in these species, and differences in amenamevir efficacy for viral kinetics between species.

The categories for lesion scores in human were not determined in the clinical study protocol, and I originally defined four categories as shown in the present study. Scores in humans showed monotonical change, i.e. the scores started from 3 and decreased along

with the lesion healing. Assuming that most patients showed lesion healing without recurrence and therefore the lesion scores tended to monotonically decrease, the definition of lesion scores seem acceptable for modeling purposes. I did not include data from patients whose lesion scores remained 0 throughout the study period (aborted lesion) in the model analysis because for a patient whose lesion score was 0 during the study, as I was unable to determine whether or not the lack of any symptoms was due to the drug's effects. Therefore, the PD model of the present analysis was built only for patients who developed the symptoms.

Finally, the lesion scores in guinea pig and human could be explained by the similar models including with two fixed-effect parameters, i.e. amount of virus plaques and the elapsed time. Previous study regarding virus plaques showed that the continual exposure of amenamevir above a certain concentration is necessary to prevent the virus re-production [32], and this was confirmed by another study with multiple dose design which is usually used in the antibiotics area [49]. During the clinical development of amenamevir, the value for EC_{50} obtained in the non-clinical studies could be directly extrapolated into the clinical study and is used for the dose rationale [30,32]. As results, the non-clinical EC_{50} without a cure effect was under-estimated, I was unable to detect a clear dose relationship in the clinical study.

In the present study, I developed similar PK/PD models in both guinea pigs and humans with Virus Plaque and Time components to explain the time-course profiles of lesion scores. A virtual kinetic profile of virus plaque was incorporated into the model in order to connect the PK profile of amenamevir with the lesion score profiles, and the terms in the logistic model consisting of the number of virus plaques and the elapsed time well explained the dose- and time-dependent PD profiles. These results suggest that the virtual number of virus plaques can be used as a built-in biomarker.

While the fixed effect in Eff of Virus Plaque was negative in both species, the fixed effect in Eff of the Time component for the immune system was negative in guinea pigs but positive in humans. HSV-2 damages the central nervous system, which in turn affects the immune system [50]. Present findings suggest that the immune system might be weakened by virus infection in guinea pigs, although evidence for this is insufficient at present. The differences in results for the Time Component between species may have been due to the different experimental conditions and different responses of immune systems. In the guinea pig study, animals were infected with a lethal amount of HSV to ensure herpes infection, and lesion severity increased with time. In humans, the immune system may work adequately to reduce lesion severity.

The effect of the Virus Plaque component was deemed to be large in guinea pigs, as efficacy was clearly dose-dependent in the amenamevir groups while the effect was saturated in the placebo group. In contrast, the effect of the Virus Plaque component was relatively small in humans, and the drug effect for lesion scores was smaller than in guinea pigs.

In humans, the PD effect was almost dose-independent, and immune system-related healing was likely the driving force behind reductions in lesion scores. These findings suggest that the drug effect may be masked in diseases healed by the immune response, such as genital herpes. Therefore, the PK/PD model proposed in the present study will be particularly useful for explaining the PK/PD relationship of drugs used to treat self-cured diseases. In antibiotics and antiviral drug kinetic analyses, drug-bacteria (or virus) interaction is assumed to be independent of *in vivo* conditions, such as host species. Here, I assumed that the kinetic parameters for virus plaque data obtained in *in vitro* experiments could be applied to both guinea pigs and humans. In addition, as a practical problem, I

cannot obtain the virus kinetic data in human and the difference of it between the species is difficult to be evaluated.

In the development of drugs for diseases with natural healing, if healing does not happen in the animal disease model, its efficacy may differ from clinical efficacy.

In the non-clinical studies from the perspective of the prediction of efficacy, animal model without natural healing which can confirm the drug power clearly is suitable, however, it may misjudge the clinical endpoint. For example, even when the development of animal models, natural healing should be considered.

2.2.5 Conclusions

This PK/PD modeling approach based on bi-directional translational approach is useful for not only new candidate exploration in the non-clinical stage but also further application in clinical data analysis. I believe that this kind of modeling and simulation approach will give some suggestions especially as a unique PK/PD modeling approach connecting the non-clinical and clinical data during the HSV drug development.

2.2.6 Figures

a)

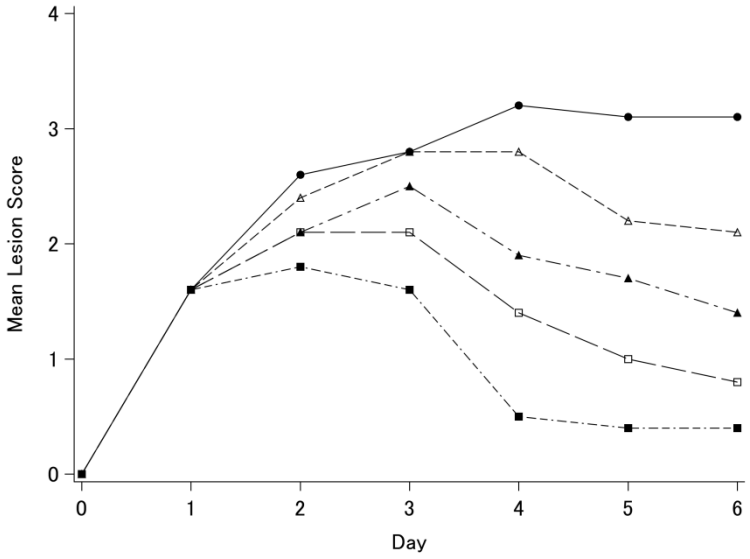

b)

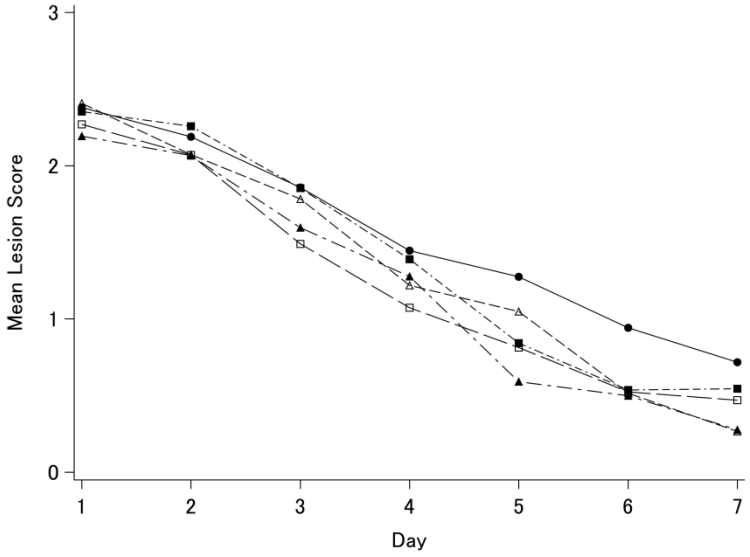

Figure 2-2- 1 Time course profiles of mean observed lesion scores in guinea pigs (a) and humans (b)

(a) Closed circle: Placebo, open triangle: 1 mg/kg, closed triangle: 3 mg/kg, open square: 10 mg/kg, closed square: 30 mg/kg; treatment duration was 5 days from Day 1. (b) Closed circle: Placebo, open triangle: 100 mg, closed triangle: 200 mg, open square: 400 mg, closed square: 1200 mg; treatment duration was 3 days from Day 1.

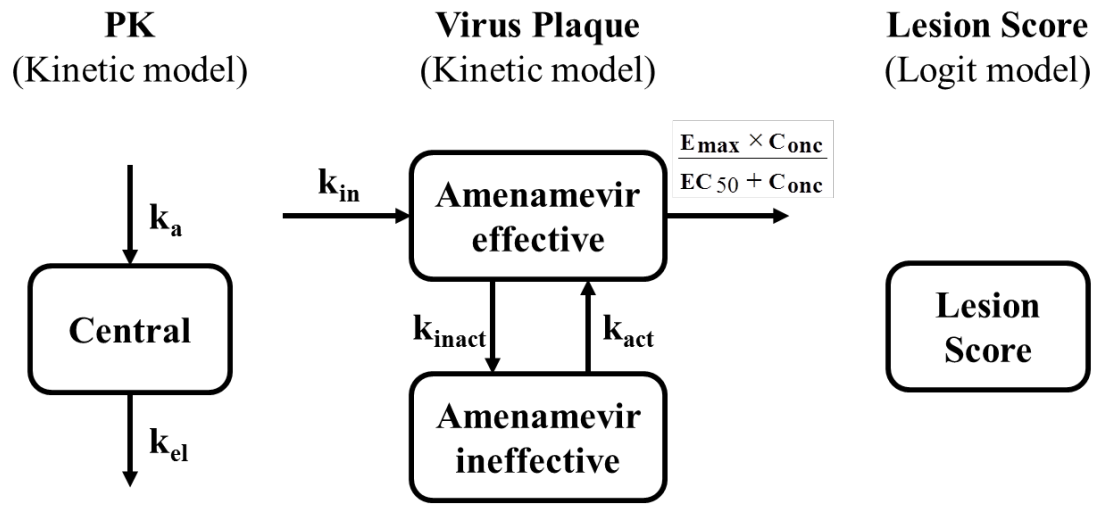

Figure 2-2- 2 Overview of the PK/PD model

a)

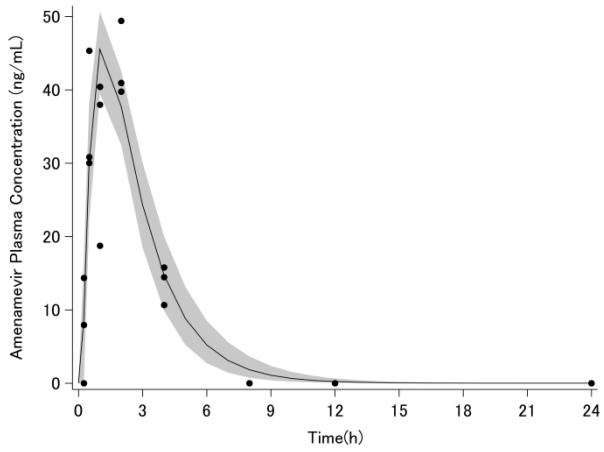

b)

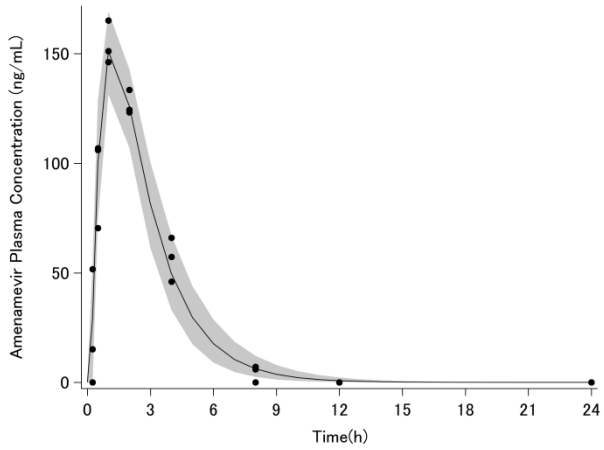

c)

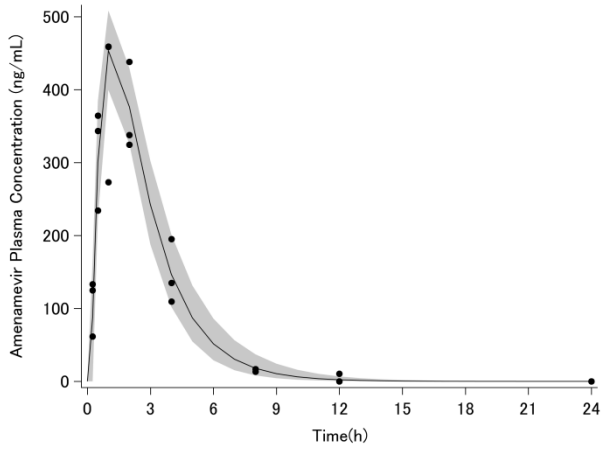

Figure 2-2- 3　Results of population PK modeling and visual predictive check in guinea pigs

(a) Dose = 0.3 mg/kg, (b) 1.0 mg/kg, (c) 3.0 mg/kg. Solid line: median, filled region: 95% prediction interval.

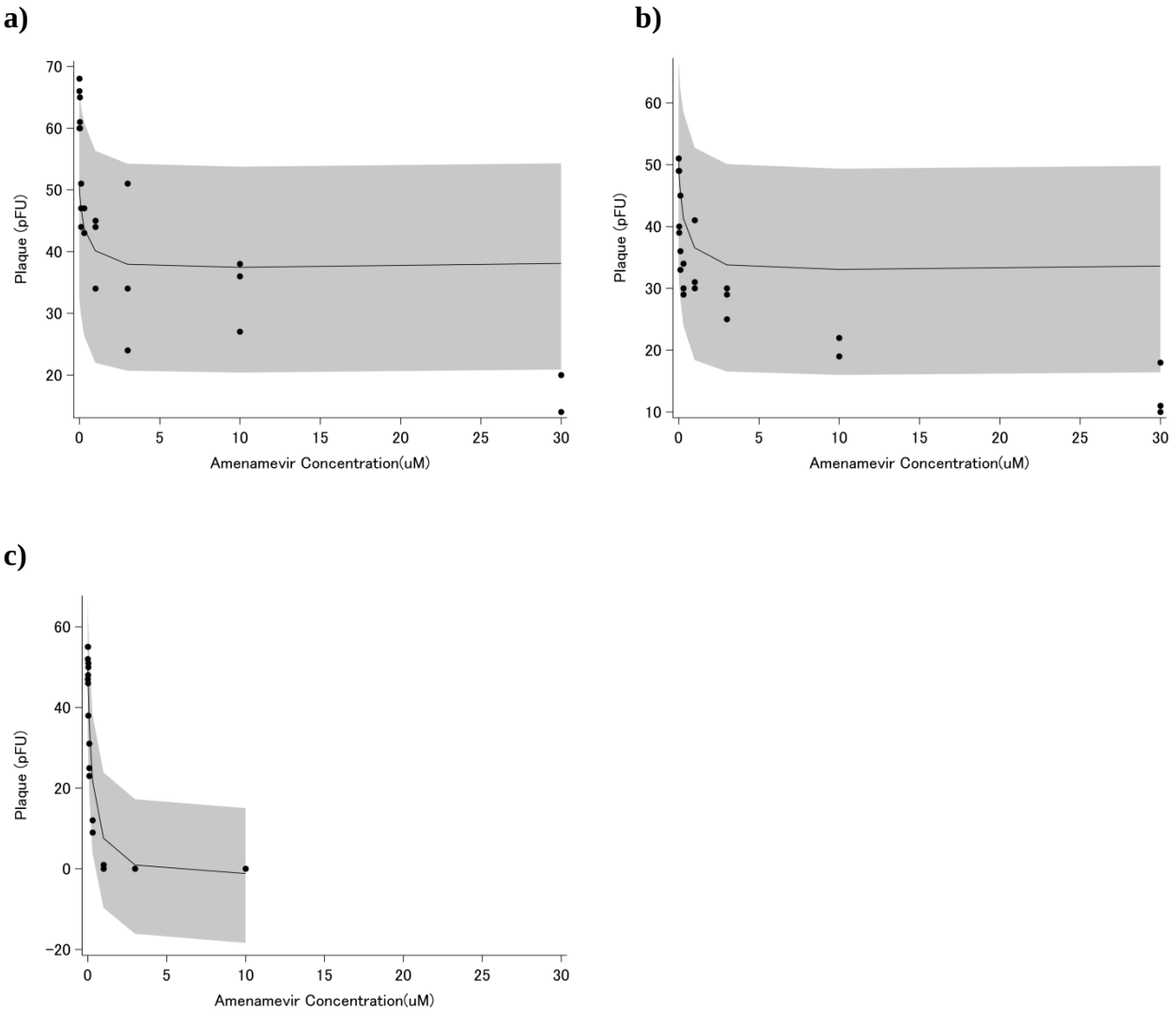

Figure 2-2- 4　Results of population PD modeling and visual predictive check for virus plaque data

(a) Amenamevir duration time = 6 h, (b) 8 h, (c) 24 h. Solid line: median, filled region: 95% prediction interval.

a)

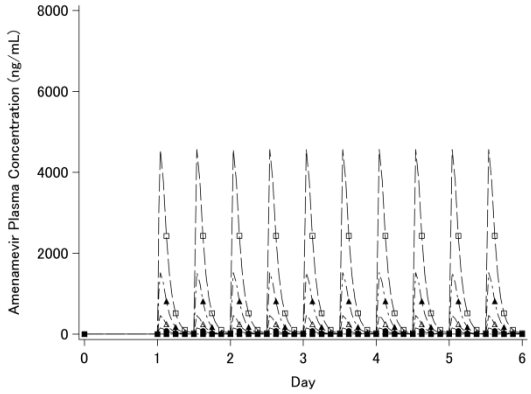
Amenamevir Plasma Concentration (ng/mL)
8000
6000
4000
2000
0
0 1 2 3 4 5 6
Day

b)

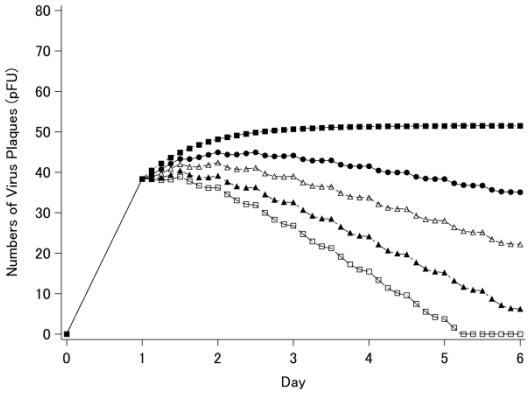
Numbers of Virus Plaques (pFU)
80
70
60
50
40
30
20
10
0
0 1 2 3 4 5 6
Day

c)

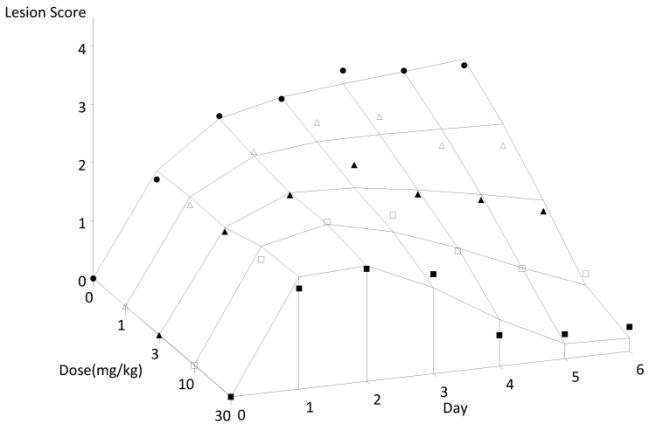
Lesion Score
4
3
2
1
0
0
1
3
10
30
Dose(mg/kg)
0 1 2 3 4 5 6
Day

d)

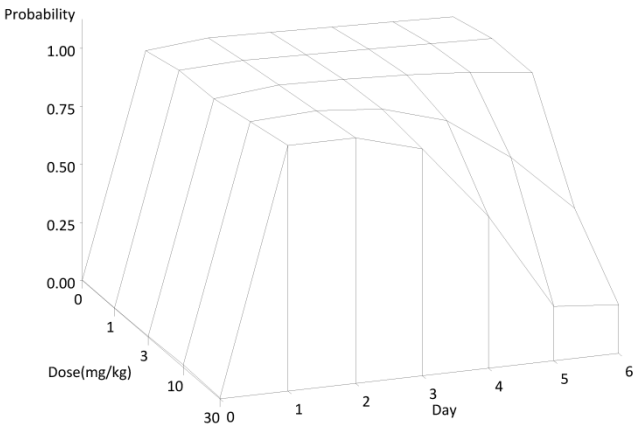
Probability
1.00
0.75
0.50
0.25
0.00
0
1
3
10
30
Dose(mg/kg)
0 1 2 3 4 5 6
Day

e)

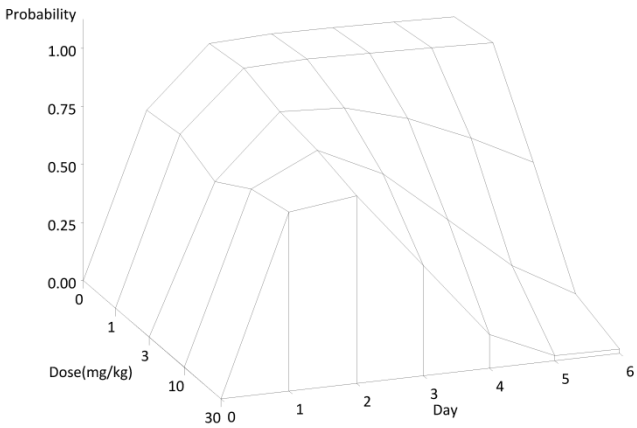
Probability
1.00
0.75
0.50
0.25
0.00
0
1
3
10
30
Dose(mg/kg)
0 1 2 3 4 5 6
Day

f) **g)**

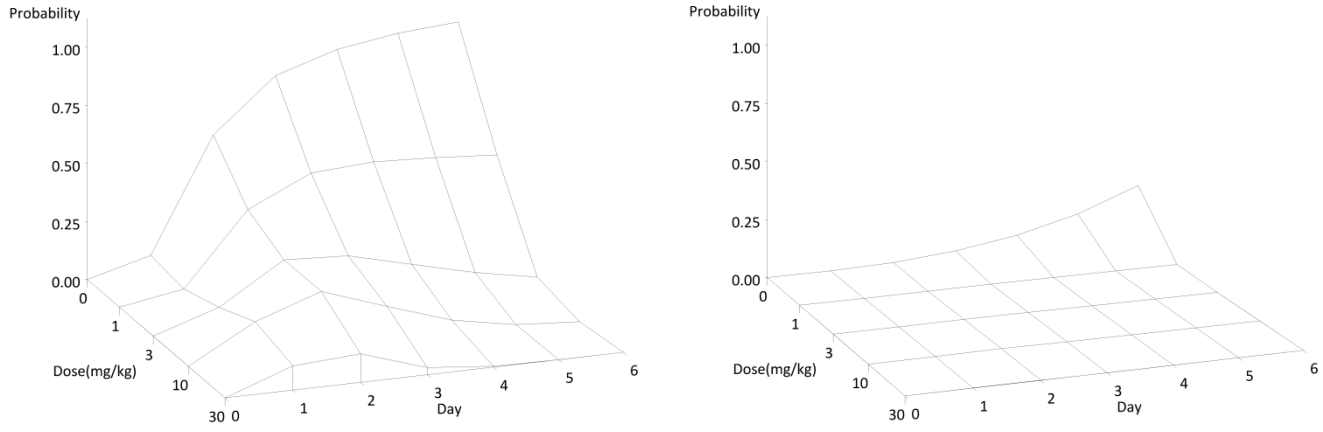

Figure 2-2- 5 Results of model predicted time course profiles in guinea pigs

Closed circle: Placebo, open triangle: 1 mg/kg, closed triangle: 3 mg/kg, open square: 10 mg/kg, closed square: 30 mg/kg; treatment duration was 5 days from Day 1. (a), (b) Simulated time-course profiles of plasma concentration and virus plaque. (c) Observed (plots) and model-predicted (lines) time-course profiles of lesion scores in guinea pigs. Predictions are given as surface of lesion scores (*z*-axis) as a function of time (*x*-axis) and dose (*y*-axis). Symbols show the observed values. (d) to (g) Predicted probability surfaces for lesion scores (*z*-axis) as a function of day (*x*-axis) and dose (*y*-axis) in guinea pigs. (d) Pr{Y>=1}, (e) Pr{Y>=2}, (f) Pr{Y>=3}, (g) Pr{Y=4}.

a)

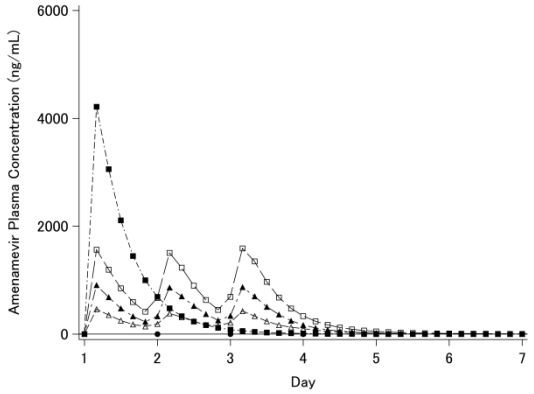
Amenamevir Plasma Concentration (ng/mL)
6000
4000
2000
0
1
2
3
4
5
6
7
Day

b)

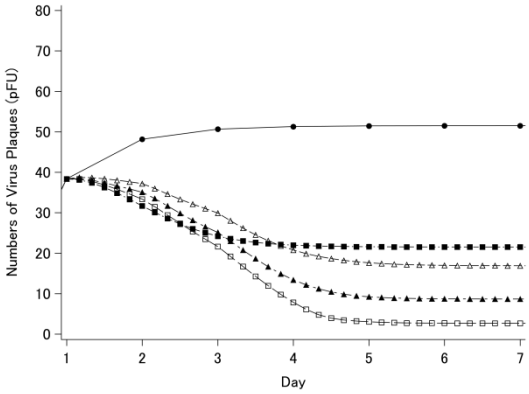
Numbers of Virus Plaques (pFU)
80
70
60
50
40
30
20
10
0
1
2
3
4
5
6
7
Day

c)

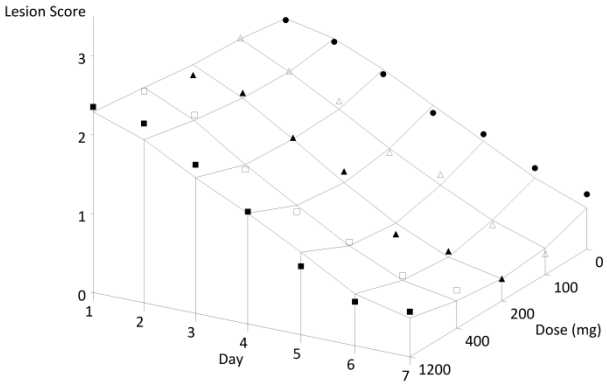
Lesion Score
3
2
1
0
1
2
3
4
5
6
7
Day
0
100
200
400
1200
Dose (mg)

d)

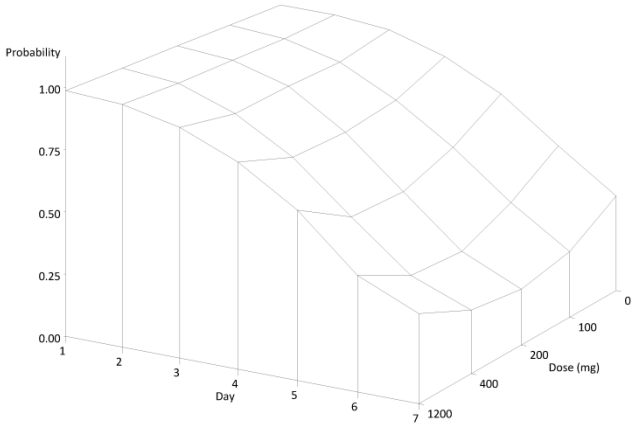
Probability
1.00
0.75
0.50
0.25
0.00
1
2
3
4
5
6
7
Day
0
100
200
400
1200
Dose (mg)

e)

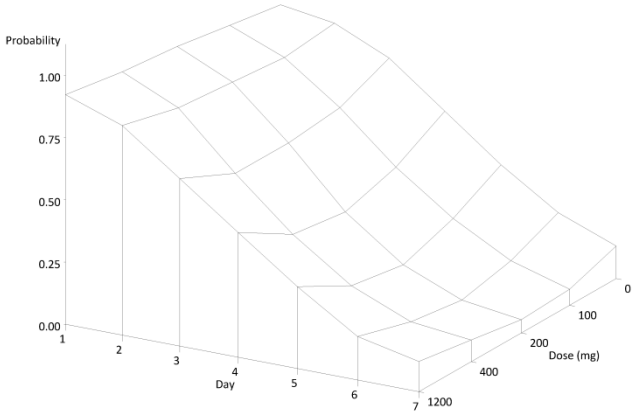
Probability
1.00
0.75
0.50
0.25
0.00
1
2
3
4
5
6
7
Day
0
100
200
400
1200
Dose (mg)

f)

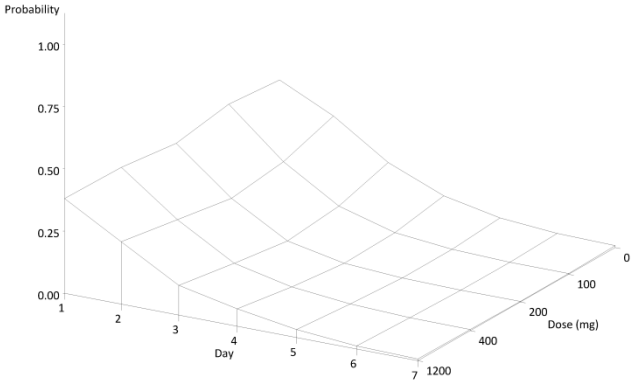

Figure 2-2- 6 Results of model predicted time course profiles in humans.

Closed circle: Placebo, open triangle: 100 mg, closed triangle: 200 mg, open square: 400 mg, closed square: 1200 mg; treatment duration was 3 days from Day 1. (a), (b) Simulated time-course profiles of plasma concentration and virus plaque. (c) Observed (plots) and model-predicted (lines) time-course profiles of lesion scores in humans. Predictions are given as surface of lesion scores (*z*-axis) as a function of time (*x*-axis) and dose (*y*-axis). Symbols show the observed values. (d) to (f) Predicted probability surfaces for lesion scores (*z*-axis) as a function of day (*x*-axis) and dose (*y*-axis) in human. (b) Pr{Y>=1}, (c) Pr{Y>=2}, (d) Pr{Y=3}.

2.2.7 Tables

Table 2-2- 1 Estimated Population parameters of Amenamevir in a guinea pig PK model and Virus Plaque PD model

Model	Parameter	Estimate (%RSE[a])	95% CI[b] (Lower – Upper)
PK model for Guinea pig	CL/F (L/h/kg)	2.04 (2.76%)	1.93 – 2.15
	V/F (L/kg)	3.89 (11.1%)	3.05 – 4.73
	ka (h^{-1})	1.76 (21.4%)	1.02 – 2.50
	Lag Time (h)	0.179 (7.15%)	0.154 – 0.204
	$\eta_{CL/F}$ (CV%)	10.7 (35.3%)	5.9 – 14.0
	η_{ka} (CV%)	14.5 (33.1%)	8.61 – 18.6
	$\eta_{lagtime}$ (CV%)	21.4 (41.6%)	9.2 – 28.9
	ε^c	9.76 (35.9%)	5.3 – 12.7
PD model for Virus Plaque（Common parameters in Guinea pigs and humans）	k_{inact} (h^{-1})	29.5 (27.6%)	13.6 – 45.4
	k_{act} (h^{-1})	179 (19.0%)	112 –246
	k_{in} (h^{-1})	0.0569 (Fixed)	–
	Emax (pFU)	0.874 (6.40%)	0.764 – 0.984
	EC_{50} (ng/mL)	127 (24.8%)	65.3 – 189
	ε^c	8.75 (18.7%)	7.0 – 10.2

CI: confidence interval, CL/F: oral clearance, V/F: volume of distribution, k_a: absorption rate, η: inter-individual variability, ε: intra-individual variability, k_{inact}: inactivation ratio , k_{act}: activation ratio, k_{in}: increase ratio , E_{max}: maximum drug effect, EC_{50}: Michaelis constant

a: %RSE is percent relative standard error (100% × Standard Error / Estimate)

b: 95% CI = T ± 1.96 × Standard Error

c: given as standard deviation

Table 2-2- 2 Estimated parameters of the logistic regression model for lesion score in guinea pigs and humans

Parameter	Guina pig		Human	
	Estimate (%RSE[a])	95% CI[b] (Lower – Upper)	Estimate (%RSE[a])	95% CI[b] (Lower – Upper)
β_1	-0.265 (10.6%)	-0.320 -0.210	-0.0247 (29.5%)	-0.0390, -0.0104
β_2	-0.0334 (14.6%)	-0.0430, -0.0238	0.0424 (6.0%)	0.0374, 0.0474
$\theta_{Score=0}$	6.76 (15.4%)	4.72, 8.80	-5.21 (6.8%)	-5.90, -4.52
$\theta_{Score=1}$	3.11 (13.2%)	2.30, 3.92	1.86 (7.3%)	1.60, 2.12
$\theta_{Score=2}$	4.17 (11.2%)	3.25, 5.09	3.34 (6.0%)	2.94, 3.74
$\theta_{Score=3}$	5.89 (12.4%)	4.46, 7.32		
η[c]	1.62 (31.7%)	0.996, 2.07	1.36 (16.2%)	1.12, 1.56

CI: confidence interval, β_1: effect of virus plaque, β_2: time effect for healing, $\theta_{Score=x}$: logit value for score x, η: inter-individual variability

a: %RSE is percent relative standard error (100% × Standard Error / Estimate)

b: 95% CI = T ± 1.96 × Standard Error

c: given as standard deviation

3 OVERALL CONCLUSION

In the present study, the relationship between pharmacokinetics and efficacy of drugs depend on the duration time was quantitatively evaluated by mathematical model using results of nonclinical studies and clinical trials.

From the results shown in Chapter 1, it became clear that depending on experimental conditions, whether efficacy of ECyd depends on concentration or on time. The importance of designing carriers for antitumor drugs based on PK model has been clarified.

From the results shown in Chapter 2, pharmacokinetics of Amenamevir in genital herpes patients was evaluated by PPK analysis. Additionally, the time dependency of Amenamevir efficacy was examined, as the reason why dose dependence of efficacy in clinical trials was not clarified, it was thought that the effect of cure by immune system was large. Furthermore, it is important for bridging research to appropriately evaluate the gap between nonclinical and clinical study became clear for the drug development in the therapeutic area where spontaneous cure is observed.

From the results shown in Chapter 2, I evaluated the pharmacokinetics of Amenamevir in genital herpes patients, examined the time dependency of efficacy, and as a reason why dose dependence of efficacy in clinical trials was not clarified, It was thought that it was thought as a factor that the effect of cure by immunization against the effect of the effect was large, and furthermore, in drug development in a disease where spontaneous cure is observed, it is important for bridging research to appropriately evaluate the gap between nonclinical and clinical study became clear.

As a result of this research, in order to properly bridge the results of *in vitro* and in vivo and clinical study from a scientific point of view, a modeling and simulation approach centered on the construction of PK model and PD model was shown to be a useful technique.

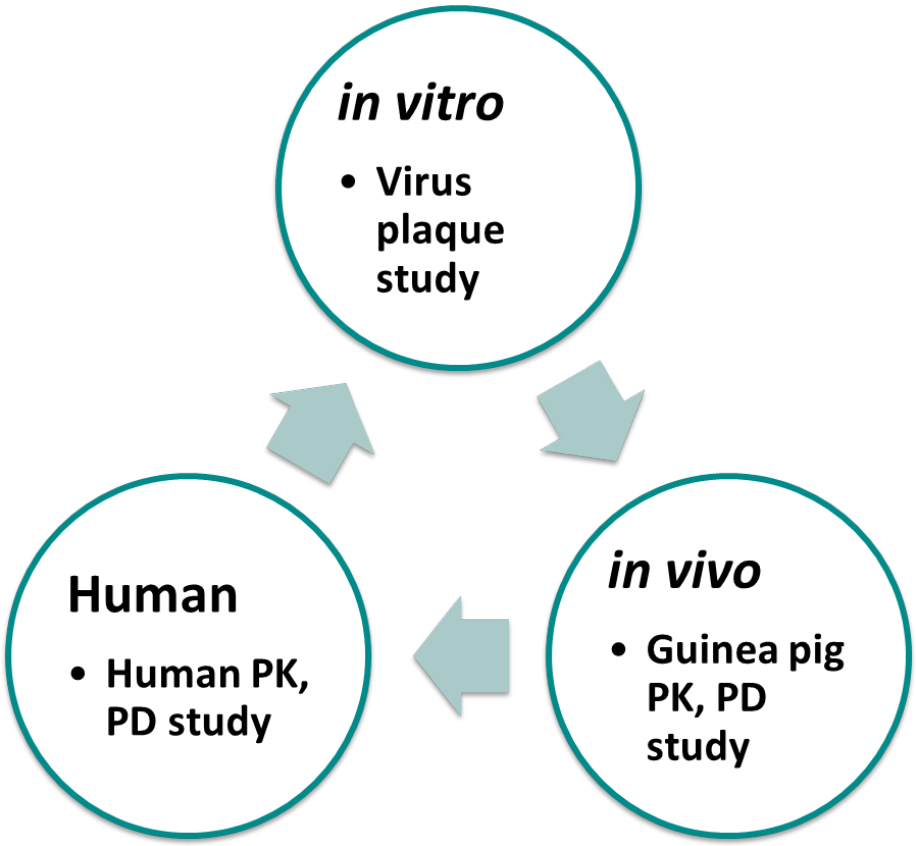

Summary figure Concept of Translational approach

4 REFERENCE

1. Shimoyama M. Cytocidal action of anticancer antigens: evaluation of the sensitivity of cultured animal and human cancer cells. *Bibl Haematol.* 1975(40):711-722.
2. Ozawa S, Sugiyama Y, Mitsuhashi J, Inaba M. Kinetic analysis of cell killing effect induced by cytosine arabinoside and cisplatin in relation to cell cycle phase specificity in human colon cancer and Chinese hamster cells. *Cancer Res.* 1989;49(14):3823-3828.
3. Ozawa S, Sugiyama Y, Mitsuhashi Y, Kobayashi T, Inaba M. Cell killing action of cell cycle phase-non-specific antitumor agents is dependent on concentration--time product. *Cancer Chemother Pharmacol.* 1988;21(3):185-190.
4. Blume G, Cevc G. Liposomes for the sustained drug release in vivo. *Biochim Biophys Acta.* 1990;1029(1):91-97.
5. Klibanov AL, Maruyama K, Torchilin VP, Huang L. Amphipathic polyethyleneglycols effectively prolong the circulation time of liposomes. *FEBS Lett.* 1990;268(1):235-237.
6. Allen TM, Hansen C, Martin F, Redemann C, Yau-Young A. Liposomes containing synthetic lipid derivatives of poly(ethylene glycol) show prolonged circulation half-lives in vivo. *Biochim Biophys Acta.* 1991;1066(1):29-36.
7. Papahadjopoulos D, Allen TM, Gabizon A, et al. Sterically stabilized liposomes: improvements in pharmacokinetics and antitumor therapeutic efficacy. *Proc Natl Acad Sci U S A.* 1991;88(24):11460-11464.
8. Vaage J, Donovan D, Mayhew E, Uster P, Woodle M. Therapy of mouse mammary carcinomas with vincristine and doxorubicin encapsulated in sterically stabilized liposomes. *Int J Cancer.* 1993;54(6):959-964.
9. Hattori H, Tanaka M, Fukushima M, Sasaki T, Matsuda A. Nucleosides and nucleotides. 158. 1-(3-C-ethynyl-beta-D-ribo-pentofuranosyl)-cytosine, 1-(3-C-ethynyl-beta-D-ribo-pentofuranosyl)uracil, and their nucleobase analogues as new potential multifunctional antitumor nucleosides with a broad spectrum of activity. *J Med Chem.* 1996;39(25):5005-5011.
10. Tabata S, Tanaka M, Endo Y, Obata T, Matsuda A, Sasaki T. Anti-tumor mechanisms of 3'-ethynyluridine and 3'-ethynylcytidine as RNA synthesis inhibitors: development and characterization of 3'-ethynyluridine-resistant cells. *Cancer Lett.* 1997;116(2):225-231.
11. Takatori S, Kanda H, Takenaka K, et al. Antitumor mechanisms and metabolism of the novel antitumor nucleoside analogues, 1-(3-C-ethynyl-beta-D-ribo-pentofuranosyl)cytosine and 1-(3-C-ethynyl-beta-D-ribo-pentofuranosyl)uracil. *Cancer Chemother Pharmacol.* 1999;44(2):97-104.
12. Takatori S, Tsutsumi S, Hidaka M, et al. The characterization of cell death induced by 1-(3-C-ethynyl-beta-D-ribo-pentofuranosyl) cytosine (ECyd) in FM3A cells. *Nucleosides Nucleotides.* 1998;17(8):1309-1317.
13. Shimamoto Y, Kazuno H, Murakami Y, et al. Cellular and biochemical mechanisms of the resistance of human cancer cells to a new anticancer ribo-nucleoside, TAS-106. *Jpn J Cancer Res.* 2002;93(4):445-452.
14. Shimamoto Y, Koizumi K, Okabe H, et al. Sensitivity of human cancer cells to the new anticancer ribo-nucleoside TAS-106 is correlated with expression of uridine-cytidine kinase 2. *Jpn J Cancer Res.* 2002;93(7):825-833.
15. Tsuchihashi M, Harashima H, Kiwada H. Development of a pharmacokinetic/pharmacodynamic (PK/PD)-simulation system for doxorubicin in long circulating liposomes in mice using peritoneal P388. *J Control Release.* 1999;61(1-2):9-19.
16. Harashima H, Iida S, Urakami Y, Tsuchihashi M, Kiwada H. Optimization of antitumor effect of liposomally encapsulated doxorubicin based on simulations by pharmacokinetic/pharmacodynamic modeling. *J Control Release.* 1999;61(1-2):93-106.

17. Szoka F, Jr., Papahadjopoulos D. Comparative properties and methods of preparation of lipid vesicles (liposomes). *Annu Rev Biophys Bioeng.* 1980;9:467-508.
18. Dams ET, Laverman P, Oyen WJ, et al. Accelerated blood clearance and altered biodistribution of repeated injections of sterically stabilized liposomes. *J Pharmacol Exp Ther.* 2000;292(3):1071-1079.
19. Laverman P, Carstens MG, Boerman OC, et al. Factors affecting the accelerated blood clearance of polyethylene glycol-liposomes upon repeated injection. *J Pharmacol Exp Ther.* 2001;298(2):607-612.
20. Ishida T, Maeda R, Ichihara M, Irimura K, Kiwada H. Accelerated clearance of PEGylated liposomes in rats after repeated injections. *J Control Release.* 2003;88(1):35-42.
21. Ishida T, Masuda K, Ichikawa T, Ichihara M, Irimura K, Kiwada H. Accelerated clearance of a second injection of PEGylated liposomes in mice. *Int J Pharm.* 2003;255(1-2):167-174.
22. Matsuda A, Sasaki T. Antitumor activity of sugar-modified cytosine nucleosides. *Cancer Sci.* 2004;95(2):105-111.
23. Shuto S, Imamura S, Fukukawa K, Sakakibara H, Murase J. A facile one-step synthesis of phosphatidylhomoserines by phospholipase D-catalyzed transphosphatidylation. *Chem Pharm Bull (Tokyo).* 1987;35(1):447-449.
24. Endo Y, Obata T, Murata D, et al. Cellular localization and functional characterization of the equilibrative nucleoside transporters of antitumor nucleosides. *Cancer Sci.* 2007;98(10):1633-1637.
25. Stanberry L, Cunningham A, Mertz G, et al. New developments in the epidemiology, natural history and management of genital herpes. *Antiviral Res.* 1999;42(1):1-14.
26. Snoeck R, De Clercq E. New treatments for genital herpes. *Curr Opin Infect Dis.* 2002;15(1):49-55.
27. Benedetti J, Corey L, Ashley R. Recurrence rates in genital herpes after symptomatic first-episode infection. *Ann Intern Med.* 1994;121(11):847-854.
28. Katsumata K, Chono K, Sudo K, Shimizu Y, Kontani T, Suzuki H. Effect of ASP2151, a herpesvirus helicase-primase inhibitor, in a guinea pig model of genital herpes. *Molecules.* 2011;16(9):7210-7223.
29. Chono K, Katsumata K, Kontani T, et al. ASP2151, a novel helicase-primase inhibitor, possesses antiviral activity against varicella-zoster virus and herpes simplex virus types 1 and 2. *J Antimicrob Chemother.* 2010;65(8):1733-1741.
30. Tyring S, Wald A, Zadeikis N, Dhadda S, Takenouchi K, Rorig R. ASP2151 for the Treatment of Genital Herpes: A Randomized, Double-Blind, Placebo- and Valacyclovir-Controlled, Dose-Finding Study. *J Infect Dis.* 2012.
31. Field HJ, Vere Hodge RA. Recent developments in anti-herpesvirus drugs. *Br Med Bull.* 2013;106:213-249.
32. Katsumata K, Chono K, Kato K, et al. Pharmacokinetics and pharmacodynamics of ASP2151, a helicase-primase inhibitor, in a murine model of herpes simplex virus infection. *Antimicrob Agents Chemother.* 2013;57(3):1339-1346.
33. Bodsworth NJ, Crooks RJ, Borelli S, et al. Valacyclovir versus acyclovir in patient initiated treatment of recurrent genital herpes: a randomised, double blind clinical trial. International Valacyclovir HSV Study Group. *Genitourin Med.* 1997;73(2):110-116.
34. Beal L, Sheiner B. *NONMEM Users Guide* UCSF.: NONMEM Project Group; 1989.
35. Wilkins JJ. NONMEMory: a run management tool for NONMEM. *Comput Methods Programs Biomed.* 2005;78(3):259-267.
36. Wang Y. Derivation of various NONMEM estimation methods. *J Pharmacokinet Pharmacodyn.* 2007;34(5):575-593.
37. Post TM, Freijer JI, Ploeger BA, Danhof M. Extensions to the visual predictive check to facilitate model performance evaluation. *J Pharmacokinet Pharmacodyn.* 2008;35(2):185-202.
38. Corey L, Wald A, Patel R, et al. Once-daily valacyclovir to reduce the risk of transmission of genital herpes. *N Engl J Med.* 2004;350(1):11-20.

39. Wald A, Zeh J, Selke S, Ashley RL, Corey L. Virologic characteristics of subclinical and symptomatic genital herpes infections. *N Engl J Med.* 1995;333(12):770-775.
40. Wald A, Zeh J, Selke S, et al. Reactivation of genital herpes simplex virus type 2 infection in asymptomatic seropositive persons. *N Engl J Med.* 2000;342(12):844-850.
41. Griffiths P. Is viral shedding a surrogate marker for transmission of genital herpes? A discussion document. *Herpes.* 2004;11(3):66-69.
42. Reddy MB, Morcos PN, Le Pogam S, et al. Pharmacokinetic/Pharmacodynamic predictors of clinical potency for hepatitis C virus nonnucleoside polymerase and protease inhibitors. *Antimicrob Agents Chemother.* 2012;56(6):3144-3156.
43. Takada A, Katashima M, Kaibara A, Sawamoto T, Zhang W, Keirns J. Statistical analysis of Amenamevir (ASP2151) between pharmacokinetics and clinical efficacies with non-linear effect model for the treatment of Genital Herpes. *Clin. Pharmacol. Drug Dev.* 2014.
44. Miller RL, Imbertson LM, Reiter MJ, Gerster JF. Treatment of primary herpes simplex virus infection in guinea pigs by imiquimod. *Antiviral Res.* 1999;44(1):31-42.
45. Lobo ED, Balthasar JP. Pharmacodynamic modeling of chemotherapeutic effects: application of a transit compartment model to characterize methotrexate effects in vitro. *AAPS PharmSci.* 2002;4(4):E42.
46. Sheiner LB. A new approach to the analysis of analgesic drug trials, illustrated with bromfenac data. *Clin Pharmacol Ther.* 1994;56(3):309-322.
47. Liu CY, Sambol NC. Pharmacodynamic analysis of analgesic clinical trials: nonlinear mixed-effects logistic models. *J Biopharm Stat.* 1999;9(2):253-270.
48. Holford N, Heo YA, Anderson B. A pharmacokinetic standard for babies and adults. *J Pharm Sci.* 2013;102(9):2941-2952.
49. Frimodt-Moller N. How predictive is PK/PD for antibacterial agents? *Int J Antimicrob Agents.* 2002;19(4):333-339.
50. Black PH. Central nervous system-immune system interactions: psychoneuroendocrinology of stress and its immune consequences. *Antimicrob Agents Chemother.* 1994;38(1):1-6.

5 ACKNOWLEDEMENT

本研究に際し，終始御懇厚な御指導，御鞭撻および本論文の御校閲を賜りました北海道大学大学院薬学研究院　医療薬学部門　薬剤分子設計学研究室教授　原島秀吉教授に謹んで感謝申し上げます。また，ご審査賜りました菅原満教授，武隈洋准教授，および山田勇磨准教授に謹んで感謝申し上げます。

本研究の端緒を与えていただくと共に，終始御懇厚な御指導およびご助言を賜りました京都薬科大学　臨床薬学教育研究センター長　矢野義孝教授に深謝いたします。

本研究の機会を与えて下さいました，アステラス製薬株式会社　開発本部長　横田智広氏，臨床薬理部部長　澤本泰治博士，研究本部長　内田渡博士に心から感謝申し上げます。また，常日頃の議論を通じて多くの知識や示唆をいただきました臨床薬理部　片島正貴博士，および貝原徳紀博士に心から感謝いたします。

ECyd の論文執筆に多大なるご協力を頂いた，広島大学大学院医歯薬保健学研究院　基礎生命科学部門　紙谷浩之教授に心から感謝いたします。

ECyd の研究にあたり，ご支援および実りある議論にご協力いただいた北海道大学薬学研究院　創薬科学研究教育センター　バイオ医薬学部門　松田彰特任教授，および創薬科学部門　創薬有機化学研究室　周東智教授に感謝いたします。

Amenamevir の研究にあたり，ご支援および実りある議論にご協力いただいたアステラス製薬株式会社　鈴木弘博士，長野浩治博士，勝俣清光博士，および Dr. Jim Kerns に感謝いたします。また，常日頃変わらぬご支援，ご協力を頂きました同臨床薬理部の皆様に厚く御礼申し上げます。

最後に，暖かい励ましをいつも送り続けてくれた家族に感謝いたします。